ARC6 AND FTSZ ASSEMBLY: STRUCTURAL AND FUNCTIONAL CHARACTERIZATION

A Dissertation

by

MIN WOO SUNG

Submitted to the Office of Graduate and Professional Studies of
Texas A&M University
in partial fulfillment of the requirements for the degree of

DOCTOR OF PHILOSOPHY

Chair of Committee,	Andreas Holzenburg
Committee Members,	James Erickson
	Steve Lockless
	Junjie Zhang
Head of Department,	Tom McKnight

December 2017

Major Subject: Biology

ABSTRACT

Chloroplasts have to divide to maintain their numbers throughout cycles of cell division by binary fission and conduct photosynthesis and fulfill other metabolic functions that are essential to plant life. Chloroplast division is achieved by complex division machinery including contractile inner ring: Z-ring and other regulatory proteins. ARC6 is one of the key regulatory proteins which are known to stabilize or maintain Z-ring and anchor it to the inner membrane by interaction with FtsZ2. However, the underlying mechanism of this modulation is unclear to date. Here, we performed biochemical characterization of ARC6 with three complementary techniques, namely 90° light scattering, sedimentation and transmission electron microscopy. Our data have shown stromal portion of ARC6 (tARC6) affects FtsZ2 assembly without forming higher order structures, and exerts it role by FtsZ2 dynamics. Interestingly, tARC6 prevented GDP induced FtsZ2 disassembly and has shown significant effect on FtsZ2 assembly when GDP was present. 3D reconstruction was also performed to elucidate structural basis and investigate binding model with FtsZ2 protofilament and PDV2. Together, our data reveal that dimeric form of tARC6 binds to FtsZ2 filaments and prevent GDP associated FtsZ2 disassembly thereby facilitate FtsZ2 assembly.

ACKNOWLEDGEMENTS

I would like to thank my committee chair, Dr. Andreas Holzenburg, and Dr. Stan Vitha for their guidance and support throughout the research project. Dr. Holzenburg provided me opportunities to work on a project and participate in the microscopy center. I also appreciate my committee members, Dr. James Erickson, Dr. Steve Lockless and Dr. Junjie Zhang for their encouragement and supportive guidance throughout the course of my research.

Thanks also go to my classmates in my year and colleagues who have been supportive and important to me and don't need their names in print. I also want to extend my gratitude to the department faculty and staff for helping me to prepare all the paper works.

Finally, thanks to my family for their encouragement and patience.

CONTRIBUTORS AND FUNDING SOURCES

Contributors

This work was supported by a thesis committee consisting of Professor Andreas Holzenburg (advisor) and Dr. Stan Vitha (co-advisor) and Dr. James Erickson, Dr. Steve Lockless of the Department of Biology and Dr. Junjie Zhang of the Department of Biochemistry and Biophysics.

The fluorescence recovery after photobleaching data analyzed for Chapter III was provided by Professor Katherine W. Osteryoung and were conducted by Dr. Allan Terbush at the Michigan State University.

All other work conducted for the thesis was completed by the student independently.

Funding Sources

The data from Dr. Katherine W. Osteryoung was funded by National Science Foundation (NSF):, MCB-1121943 and MCB-1719376.

NOMENCLATURE

CCD	Charge-Coupled Device
cDNA	complementary DNA
DNA	deoxyribonucleic acid
DTT	dithiothreitol
EDTA	ethylenediaminetetraacetic acid
EMAN	electron micrograph analysis
GDP	guanosine diphosphate
GPCPP	guanosine-5'-[(α,β)-methyleno]triphosphate
GTP	guanosine triphosphate
HEPES	4-(2-hydroxyethyl)-1-piperazineethanesulfonic acid
IPTG	isopropyl β-D-1-thiogalactopyranoside
Ni–NTA	nickel-nitriloacetic acid
OD	optical density
PAGE	polyacrylamide gel electrophoresis
PMSF	phenyl-methylsulfonyl fluoride
RT	room temperature
SDS	sodium dodecyl sulfate
SEM	standard error of the mean
T-DNA	transfer DNA
TEM	transmission electron microscopy

Tris	tris(hydroxymethyl)aminomethane

TABLE OF CONTENTS

Page

LIST OF FIGURES

Page

LIST OF TABLES

Page

CHAPTER I

INTRODUCTION

1.1 INTRODUCTION TO PLASTID DIVISION

Chloroplasts host photosynthesis and fulfill other metabolic functions that are essential to plant life [1-3]. Similar to their cyanobacterial ancestors, chloroplasts have to divide to maintain their numbers throughout cycles of cell division by binary fission [1, 4]. Due to their endosymbiotic origin, the division machineries of chloroplasts and all plastids share some core similarities with the bacterial division apparatus [5]. Recent studies have revealed that plastid division is accomplished by concentric contractile rings at the midpoint of plastid comprised of Filamenting temperature-sensitive mutant Z (FtsZ) ring on the stromal side of inner envelope membrane (IEM) and Accumulation and Replication of Chloroplasts 5 (ARC5/Dynamin-Related Protein 5B (DRP5B) ring on cytosolic side of outer envelope membrane (OEM) that function. Overall plastid division process is shown in Figure 1-1.

In algae and plants, two conserved FtsZ families are encoded, FtsZ1 and FtsZ2 that arose by gene duplication and divergent evolution from the single FtsZ gene of the cyanobacterial endosymbiont [6-8]. FtsZ1 and FtsZ2, tubulin-like GTPase proteins [9], form filaments in the mid-cell and anchored to inner-membrane by a protein named the Accumulation and Replication of Chloroplasts 6 (ARC6) which interacts specifically with FtsZ2 [5, 10]. Downstream of ARC6, possible alternative membrane anchoring

protein Paralog of ARC6 (PARC6) was known to act at the division site [11] through interaction with conserved C-terminal tail of FtsZ2 [12].

Localization of Z-ring in the mid-cell is regulated by Minicell D1 (MinD1) and Minnicell E1 (MinE1) which function through Accumulation and Replication of Chloroplasts 3 (ARC3), and ARC3 mediates division-site placement by inhibiting Z-ring assembly primarily through interaction with FtsZ2 at the poles of the cell [13]. Bacterial FtsZ proteins assemble and form bundles in the middle of the cell by Min CDE system [14]. Bacterial MinD is a membrane associated protein recruiting MinC upon ATP binding and forms MinC-MinD complex structure at the polar zone inhibiting FtsZ assembly [15-18]. Chloroplast MinE1 stimulates ATPase of MinD1 [19] as bacterial MinE which is known to release MinD from the membrane by stimulating ATPase activity of MinD [20-22]. Plant-specific protein Multiple Chloroplast Division site 1 (MCD1) is also known to be required for MinD localization to regulate FtsZ ring formation and positioning in *Arabidopsis thaliana* chloroplasts [23]. Once ARC6 mediated Z-ring formed at the middle of the plastid, MCD1, MinD1, MinE1 are recruited to the division site prior to the constriction [3, 23, 24].

Outer ring is constituted by glycosyltransferase protein plastid-dividing ring 1 (PDR1) which constructs the PD ring [25] and ARC5, a dynamin like GTPase protein which is recruited by transmembrane OEM proteins, Plastid division 1 (PDV1) and Plastid division 2 (PDV2) [26]. ARC6 is known to recruit PDV2 to the midplast through direct interaction with C-terminus of PDV2 [1, 26, 27] and a recent study has shown crystal structure of it complex form [28]. PDV1 is recruited by PARC6 which is recruited to the

Z-ring downstream of ARC6 [11]. As ARC5 is recruited to the division site and forms a continuous ring, PDV1 and PDV2 together promote constriction outer ring [29]. This contractile outer ring is thought to perform the final squeeze and separate chloroplast to the two daughter cells [28]. Detailed plastid division machinery is summarized in the Figure 1-2.

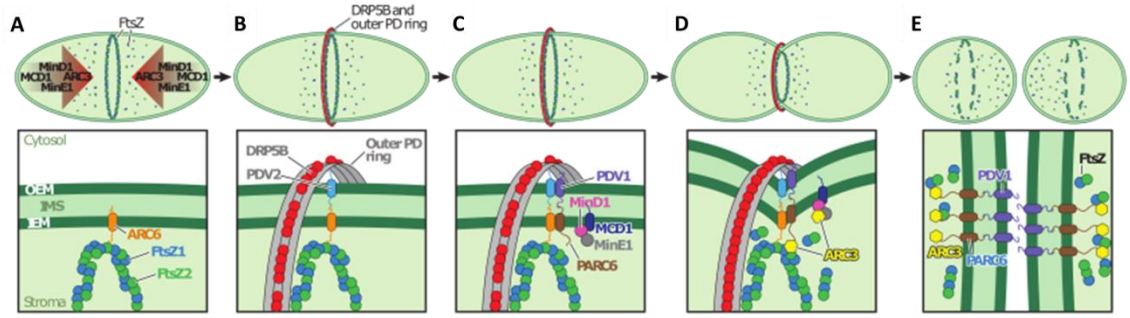

Figure 1-1. Working model of the stepwise assembly and constriction of the chloroplast division complex in higher plants. (A) Plastid division is initiated by assembly of FtsZ1 and FtsZ2 in the middle of plastid Z-ring formation is assisted and tethered to the membrane by ARC6 which is located in the inner envelope membrane [27, 30]. (B) Once Z-ring is formed, C-terminus of ARC6 interacts with C-terminus of PDV2 in the intermediate space and PDV2 recruits DRP5B [29]. The outer PD ring is constructed before the recruitment of DRP5B-ring [31]. (C) Downstream of ARC6 mediated Z-ring formation, PARC6 is recruited to the Z-ring [11] and interact with PDV1 which is also located in the outer envelope membrane and recruit DRP5B as PDV2 [29]. MCD1, MinD1, MinE1 are recruited to the division site prior to the constriction [3, 15, 23]. (D) PDV1 and PDV2 together promote constriction of DRP5B ring [29]and ARC3 is recruited to the division site by direct interaction with PARC6 and promote remodeling of FtsZ proteins [32]. (E) Immediately following separation of the two daughter chloroplasts, PDV1 and PARC6 were detected at polar site [11, 33], but ARC6 was not. Figure is adapted from previous publication [1].

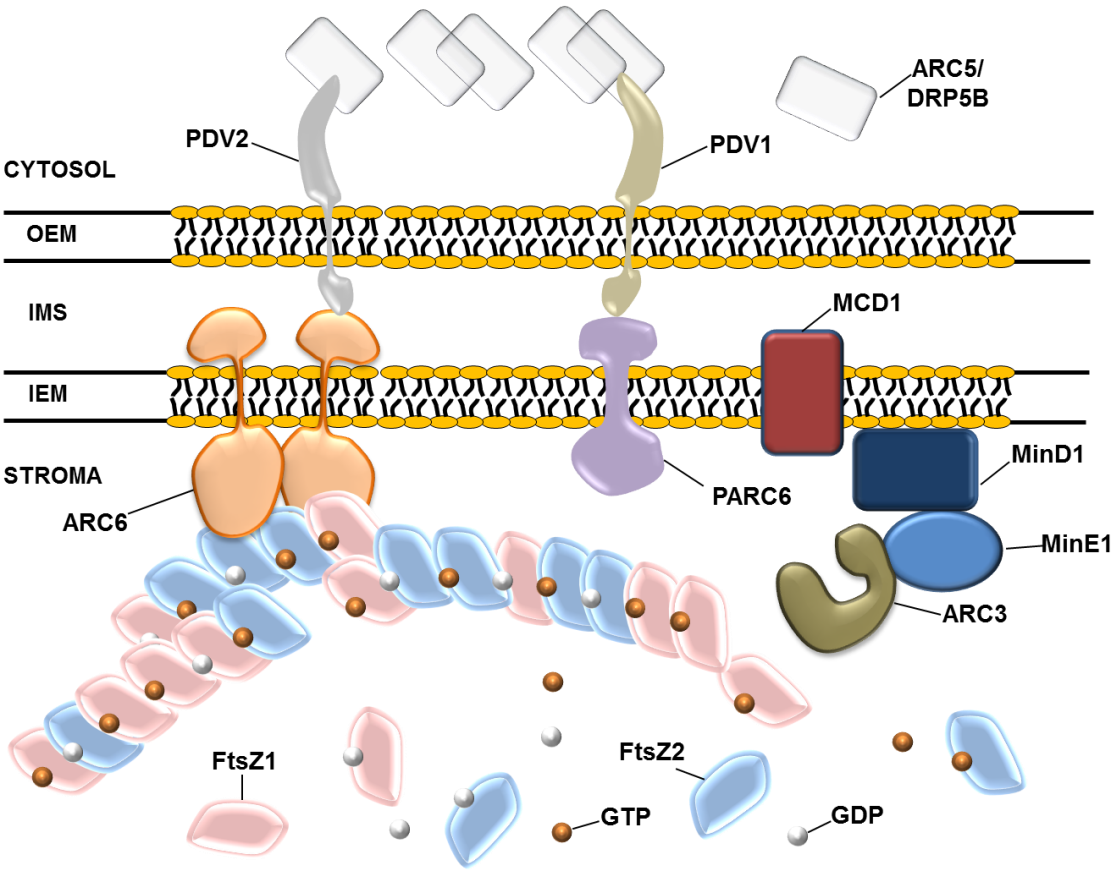

Figure 1-2. Chloroplast division machinery. The most important components and their hypothetical arrangement are shown. FtsZ1/FtsZ2 heteropolymers at the division site are stabilized and anchored to inner envelope membrane (IEM) via ARC6-FtsZ2 interaction. ARC3 and paralog of ARC6 (PARC6) interact to remodel or destabilize the filaments. FtsZ assembly is promoted by GTP binding. Hydrolysis of GTP causes conformational changes in FtsZ and is thought to promote filament curvature. OEM, outer envelope membrane, IEM, inner envelope membrane; IMS, intermembrane space

1.2 INTRODUCTION OF THE DIVISION MACHINERY: FTSZ2 AND ARC6

Most of what we know about plastid division (PD) has been guided by researches in bacterial cell division. Bacteria contain single ring-shaped division machinery, whose assembly is initiated by polymerization of a tubulin-like GTPase, FtsZ, into a ring (Z-ring) at mid-cell [34]. And the Z-ring recruits additional components to assemble functional division machinery and to remodel the peptidoglycan cell wall [35, 36]. It is known that bacterial FtsZ proteins require guanosine nucleotide binding for assembly [37] and GTP binding on FtsZ initiates monomer-monomer interactions and hydrolyze GTP by association of two FtsZ monomers [38]. Dimeric FtsZ lose some of association upon GTP hydrolysis and generate curvature [39, 40]. The same model of transition to curvature upon GTP hydrolysis was suggested from crystal structures of FtsZ [40, 41]. Similarly, chloroplast FtsZ does not require GTP hydrolysis but nucleotide binding is needed for assembly [42, 43]. FtsZ1 and FtsZ2 proteins are expected to assemble linearly into filaments in which the GTP binding site is at the axial association interface between consecutive subunits completing GTPase site [44] (Figure1-3. A-C).

In bacteria, free GDP-bound subunits exchange their nucleotide and recycle into the FtsZ polymers (Figure1-3. D), thus assembly of FtsZ within the Z-ring is dynamic with a subunit half-life on the order of tens of seconds [45-47]. In *Escherichia coli* (*E. coli*) FtsZ filament, GTP:GDP ratio in FtsZ polymer was about 50:50 for concentrations of >100μM which can lead to fractionation of the filament into shorter filaments upon GTP hydrolysis mediated disassembly [47]. On the other hand, microtubule, which is ancestral protein of FtsZ, can undergo destabilizing transition upon GTP hydrolysis on

its “GTP-cap” [48]. In case of FtsZ/tubulin-like protein TubZ filaments, disassembly occurs as treadmill like actin filaments by polymerizing at one end while depolymerizing upon GTP hydrolysis [49].

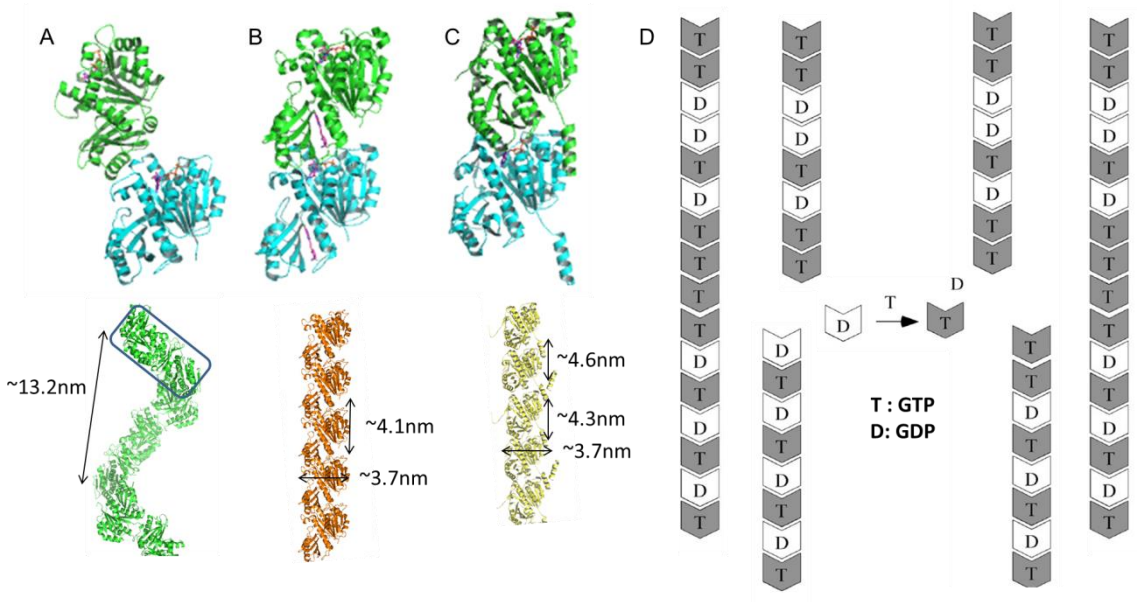

Figure 1-3. Dimeric FtsZ subunits in protofilaments and FtsZ assembly dynamics. (A-C) prokaryotic FtsZ formed dimers (upper panel) in their crystal lattices, and form helical (A) or straight (B-C) protofilaments (lower panel). Length of a pitch (A) and height and width of subunits (B-C) in protofilaments are indicated with black arrow. (A) dimeric FtsZ in a helical protofilament from *Mycobacterium tuberculosis* (PDB:1RLU). (B) dimeric Ftsz in a straight protofilament from *Staphylococcus aureus* (PDB: 4DXD). (C) dimeric FtsZ in a straight protofilament from *Methanocaldococcus jannaschii* (PDB: 1W59). (D) FtsZ protofilament include ~50 % of GTP bound subunits and fragmentation is favored at GDP subunits. GDP can be exchanged with GTP, and GTP subunit can be re-associated and protofilaments can be annealed [47].

The FtsZ sequences and proteins used in this work are of the model plant *Arabidopsis thaliana*. There, the FtsZ1 family has a single member AtFtsZ1-1 while the FtsZ2 family comprises two proteins, AtFtsZ2-1 and AtFtsZ2-2. Since AtFtsZ2-2 is redundant with AtFtsZ2-1 [25], only AtFtsZ1-1 and AtFtsZ2-1 are used and referred to as FtsZ1 and FtsZ2, respectively. FtsZ1 and FtsZ2 are functionally different and are both required for normal plastid division (Figure 1-4) [50-52].

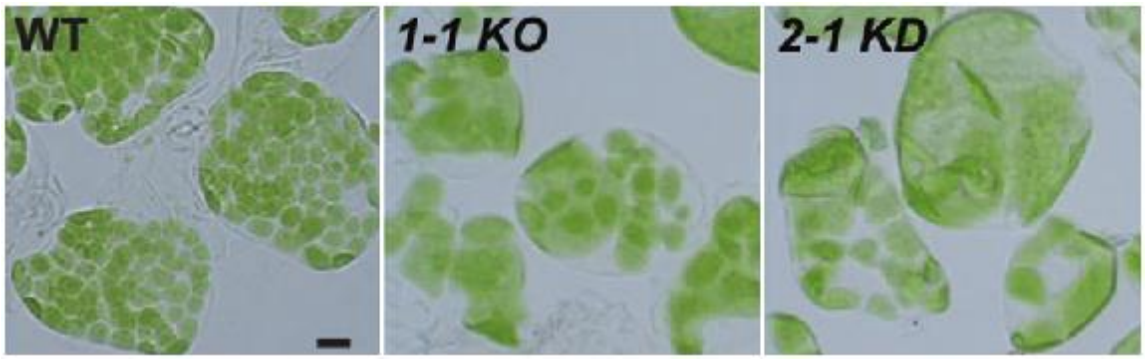

Figure 1-4. Chloroplast morphology in wild-type *Arabidopsis* and ftsZ1-1 and ftsZ2-1 T-DNA insertional mutants. Bright-field images of mesophyll chloroplast phenotypes for wild type (WT), FtsZ1-1 knock out (KO) and FtsZ2-2 knock down (KD) insertional mutants. Scale bar = 10 μm. Figure was adapted from published results [52].

FtsZ1 and FtsZ2 interact with each other to form the Z-ring structure at the division site [34, 53], and FtsZ2 seems to be primary determinant of hetero polymer morphology, while FtsZ1 may role in Z-ring modulation and remodeling [43]. The molar ratio between FtsZ1 and FtsZ2 in wild type *Arabidopsis* remained at approximately 1:2 throughout the growth [54], however, the maximum co-assembly of FtsZ1 and FtsZ2 was observed at a 1:1 stoichiometry [42]. Co-assembly of these two proteins and Z-ring

formation are modulated by accessory proteins and antagonistic regulators of Z-ring formation such as ARC6, MinD1, MinE1, ARC3 and PARC6 [11, 13, 27, 30, 55]. ARC6 is a chloroplast division protein of prokaryotic origin that arose in cyanobacteria and cyanobacterial orthologue of ARC6, Ftn2 or ZipN is found to be 22% identical and 43% similar to *Arabidopsis* ARC6 [1, 30]. The gene of arc6 was found in *Arabidopsis* mutants which have only one or two drastically enlarged chloroplasts in their leaf mesophyll cells [56] and in other cells and tissues [57, 58] suggesting that ARC6 is involved in division of all plastid types [1].

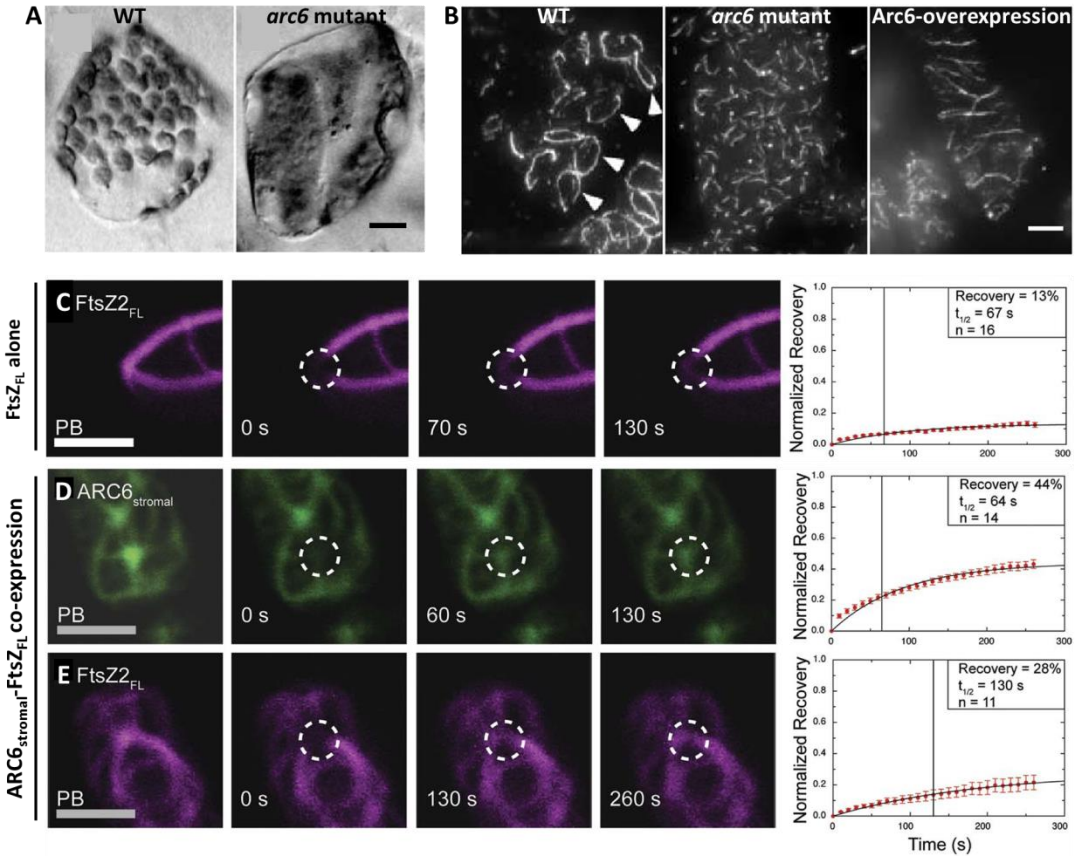

Figure 1-5. Effect of ARC6 on Z-ring formations in chloroplast. (A) Chloroplast morphology in wild-type *Arabidopsis* (WT) and arc6 mutant. (B) Immunofluorescence micrographs showing localization of fluorescence labeled FtsZ2 in leaf mesophyll chloroplasts. Wild-type (WT) chloroplasts each with a single FtsZ ring indicated by arrowheads (left), a single, enlarged arc6 mutant chloroplast (middle), and a single, enlarged chloroplast of an ARC6-overexpressing plant (right). (C-E) Steady-state polymer dynamics of the mCerulean labeled full length FtsZ2 (FtsZ2FL) alone (C) and mVenus labeled stromal portion of ARC6 co-expressed with mCerulean-FtsZ2FL (D and E respectively). (A-B) and (C) were adopted from published results [30, 59].

ARC6 is a bitopic protein localized to the inner envelope membrane (IEM) of the chloroplast, with its N-terminal portion exposed in the stroma, while the smaller C-terminal region is located in the intermembrane space [30, 60, 61]. Consistent with this topology, stromal portion of N-terminal ARC6 can interact with FtsZ2 [27, 53, 54] while C-terminal portion of ARC6 in the intermembrane has direct interaction with C-terminal peptide of PDV2 and recruit to the midplast [1, 26-28].

In the arc6 mutant chloroplasts, FtsZ filament assembly is disrupted and chloroplast division is completely blocked and instead of a single Z-ring at mid-plastid, FtsZ forms numerous very short filamentous and dot-like assemblies while Z-ring formed excessively long filaments when ARC6 is overexpressed [30] (Figure 1-5. A-B). Although the other FtsZ anchoring mechanism is present in *Arabidopsis* [61], ARC6 is thought to be an FtsZ-stabilizing factor that anchors the FtsZ filaments to the inner envelope membrane via direct interaction with FtsZ2 [27, 54, 61]. Furthermore, fluorescence protein labeled full length FtsZ2 (49-478) and N-terminal stromal portion of ARC6 (68-614) were expressed in *Schizosaccharomyces pombe* (*S. pombe*) as a heterologous expression system, and the Fluorescence Recovery After Photobleaching (FRAP) was performed showing that stromal portion of ARC6 affect dynamics of FtsZ2 by significantly reducing its turnover (Figure 1-5. C-E) [59]. This data showed that ARC6 directly stabilizes Fts2 polymers as suggested previously [30], however detailed biochemical properties and how ARC6 stabilize FtsZ2 filaments are not know up to date.

The interaction between C-terminus of ARC6 and PDV2 plays a key role in equatorial positioning of Z-ring and DRP5B-ring and coordinating localization across the two

membranes [1, 27]. Also, disruption of interaction between conserved C-terminal domain of ARC6 and C-terminus peptide of PDV2 in the intermembrane space causes abnormal division of chloroplast [27, 28]. A recent study has shown crystal structure of C-terminal domain of ARC6 and C-terminal peptide of PDV2 complex and suggested PDV2 induce ARC6 dimerization [28], however, our data revealed that stromal portion of ARC6 formed dimer in our buffer which will be described and discussed later. Ftn2 is the cyanobacterial orthologue of ARC6 and this has been reported to form dimer or oligomers [62].

ARC6 includes J-like domain missing key residues common to canonical J domains and suggested to have a function as HSP70 which is one of the representing chaperone protein including J-domain and known interact with FtsZ in *E. coli* [30]. However, ARC6 did not stimulate chloroplast HSP70 ATPase activity which indicates ARC6 is not a HSP70 like chaperone [1]. Interestingly, J-like domain of ARC6 interacts with J-like domain of Chloroplast J-like Domain 1 (CJD1) which influences fatty acid composition of chloroplast lipids in *Arabidopsis* [63]. However, the role of J-like domain in the regulation of FtsZ assembly or previously suggested self-interaction of ARC6 [53] was not known.

Molecular details of the effect ARC6 exerts on FtsZ2 assembly will aid the understanding of the mechanism of the chloroplast division apparatuses and will also open a window into the evolution of cell division.

CHAPTER II

EFFECT OF ARC6 ON FTSZ2 POLYMERIZATION

2.1 INTRODUCTION

ARC6 is localized to the inner envelope membrane of the chloroplast by its transmembrane domain (619-638) and anchors FtsZ filaments to the [30, 60, 61, 64]. ARC6 is thought to stabilize FtsZ filaments via direct interaction with C-terminal of FtsZ2 (Figure 1-2) but not with FtsZ1, which lacks the conserved C-terminal core. [27, 53, 54, 61]. In bacterial division machinery, the productive interaction of FtsZ and FtsA is known to be regulated by stoichiometric ratio of these proteins [65, 66]. Stromal portion of ARC6 were expressed with and without FtsZ proteins by the same promotor in their constructs which gave approximately same level of expression *in vivo* [12, 59]. However, ARC6 was not investigated and its biochemical properties and effect on FtsZ2 assembly *in vitro* were not elucidated up to date. To test the previously suggested role of ARC6, various truncated forms of stromal portion of ARC6 and FtsZ2 were constructed and expressed by *E. coli*. Expressed ARC6 and FtsZ2 proteins were sufficiently purified as dimers and dimeric stromal portion of ARC6 was used to investigate its effect on FtsZ2 assembly. Experiments were conducted with three complementary techniques, namely 90° light scattering, sedimentation and transmission electron microscopy which were traditionally used in bacterial FtsZ polymerization studies [67]. Our data have shown that the stromal portion of ARC6 has a dose-dependent effect on FtsZ2 assembly and unlike bacterial regulators, FtsZ2 did not form higher order structures in the presence of ARC6 *in vitro*.

2.2 RESULTS

2.2.1 Design of ARC6 and FtsZ2 constructs and purification of recombinant proteins

ARC6 structural and functional domains [30, 63] depicted in Figure 2-1, A are as follows: chloroplast transit peptide (aa 1-67), conserved stroma-localized N-terminal region (89-519) that includes the J-like domain (89-159), the transmembrane domain (615-635) that is predicted to form a single helix [30] and the conserved C-Terminal domain (679-774) located in the intermembrane space where it interacts with chloroplast division protein PDV2 [27, 28, 30]. The N-terminal region is known to interact with the key chloroplast division protein FtsZ2 [53].

In all constructs used in this study the chloroplast transit peptide and the flexible region at N-terminus (68-88) were omitted. Besides the full-length ARC6 (89-801), the chloroplast stroma-localized portion of ARC6 was used in several deletion constructs to dissect the functional roles of the individual domains. Truncated portion of ARC6 (tARC6; aa 89-519) representing the entire conserved N-terminal region was used to investigate how ARC6 affects filament assembly through interaction with FtsZ2 without tethering the filaments to the membrane. A similar construct from previous work tagged with mVenus [59] was used for in-vivo FRAP assays in *S. pombe*, also presented here. To test the role of the J-like domain of ARC6, the conserved N-terminal domain without the J-like domain was also constructed (ARC6ΔJ). The chloroplast J-like Domain 1 protein (CJD1) is known to interact with N-terminal portion of ARC6 (84-209) [63]. We hypothesized that interactions with FtsZ2 and CJD1 are facilitated by different regions

of ARC6. Therefore, two constructs spanning residues 89-310 (ARC6ΔC) and 310-519 (ARC6ΔN) were also introduced to *E. coli* for expression (Figure 2-1, A).

Full length FtsZ2-1 (FtsZ2, 49-478) construct without transit peptide (1-48) [42] included the conserved C-terminal core motif (463-478) [68-70] which is known to interact with ARC6. A truncated form of FtsZ2 (tFtsZ2, 118-424) without the flexible N and conserved C terminal domain was also constructed in order to test whether ARC6 interacts with other domains of FtsZ2 (Figure 2-1, B).

Figure 2-1. Constructs of ARC6 and FtsZ2 and effect of their expression on *Escherichia coli* Rosetta (DE3) pLysS cell morphologies. (A) ARC6 structural elements.TP: transit peptide (1-69), J-like: J-like domain (89-153), CR: conserved region (89-509), TM: transmembrane, PDV2:PDV2 binding domain (679-774). Truncated constructs include full ARC6 (89-8011), tARC6 (89-519), tARC6ΔC (89-310), tARC6ΔN (310-519), GFP-tARC6 and ARC6-mVenus (68-615) as shown. (B) Structural elements of FtsZ2 including transit peptide (TP), conserved FtsZ domain and conserved C-terminus tail as indicated. Constructs of FtsZ2 include FtsZ2 (49-476) , tFtsZ2 (118-424) and FtsZ2- or FtsZ2D322A-CFP(49-476) as shown. (C) *E. coli* cells were imaged by phase contrast before (left panel) and after overnight growth at 18 °C in the presence of 0.5 mM IPTG inducing corresponding ARC6 and FtsZ2 constructs (right panel) as indicated. Scale bar corresponds to 20 μm.

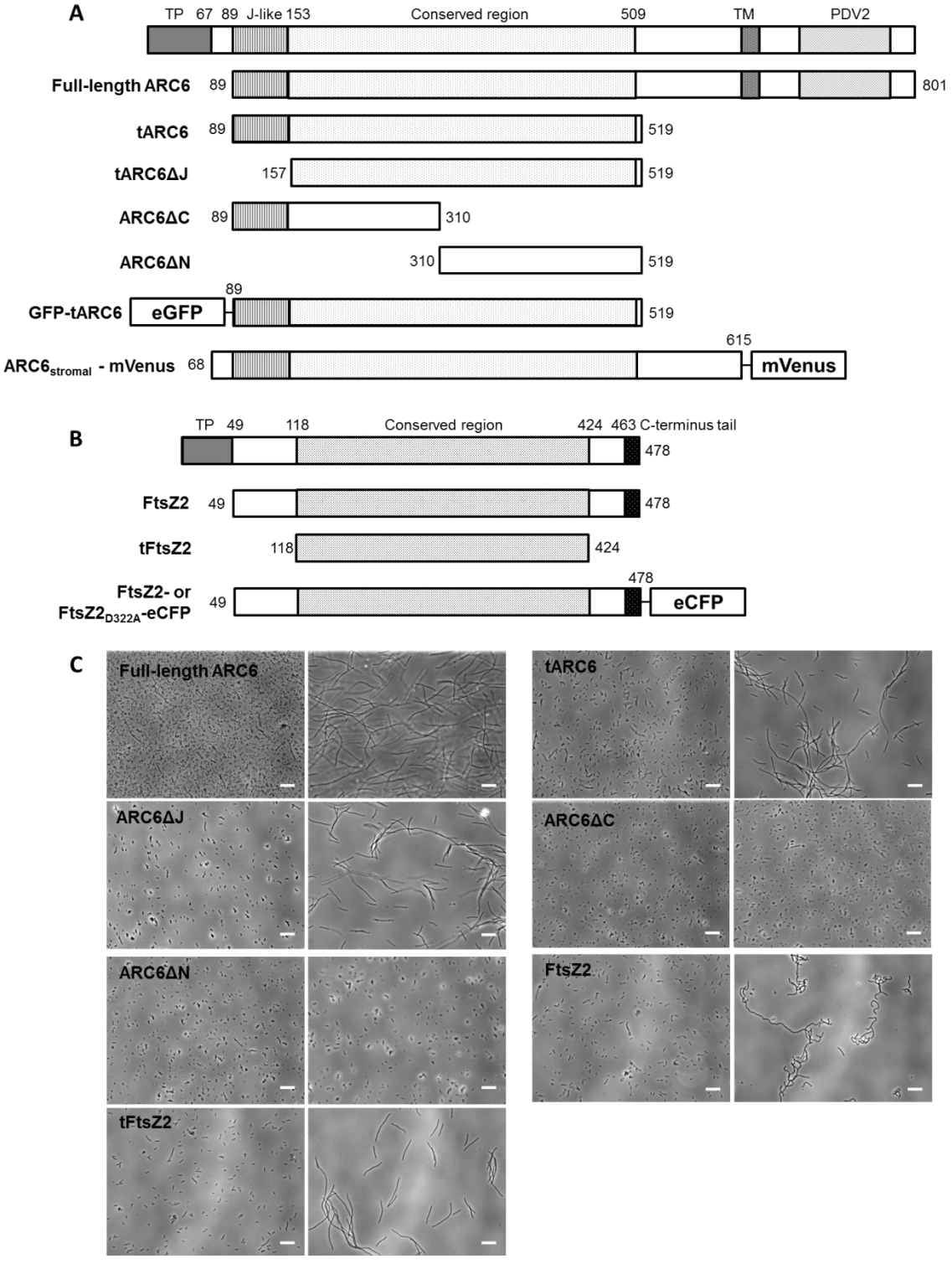
A
TP
67
89
J-like
153
Conserved region
509
TM
PDV2
Full-length ARC6
89
801
tARC6
89
519
tARC6ΔJ
157
519
ARC6ΔC
89
310
ARC6ΔN
310
519
GFP-tARC6
eGFP
89
519
ARC6stromal - mVenus
68
615
mVenus
B
TP
49
118
Conserved region
424
463
C-terminus tail
478
FtsZ2
49
478
tFtsZ2
118
424
FtsZ2- or FtsZ2D322A-eCFP
49
478
eCFP
C
Full-length ARC6
tARC6
ARC6ΔJ
ARC6ΔC
ARC6ΔN
FtsZ2
tFtsZ2

E. coli Rosetta (DE3) pLysS expression system was used for all of constructs and achieved suitable expression level and solubility leading to successful purifications of all of proteins except ARC6ΔC and ARC6ΔN which were not expressed sufficiently. Microscopic examination of bacterial cultures before and after induction indicated that with the exception of ARC6ΔC and ARC6ΔN, expression of the recombinant protein blocked bacterial cell division and caused filamentation of bacterial cells, probably through interactions with the cell division protein FtsZ that is evolutionarily and structurally related to the chloroplast division protein FtsZ2 [7]. The filamentation phenotype thus indicates that the given recombinant protein is likely to interact with the plant FtsZ2.

The tARC6 was purified as a dimer (Figure 2-2) in the buffer used for FtsZ assembly (see Methods). The dimeric form of tARC6 was confirmed by single particle analysis and 3D reconstruction described in this report. FtsZ2 and tFtsZ2 proteins were also successfully purified as dimers (Figure 2-2) consistent with published results [71].

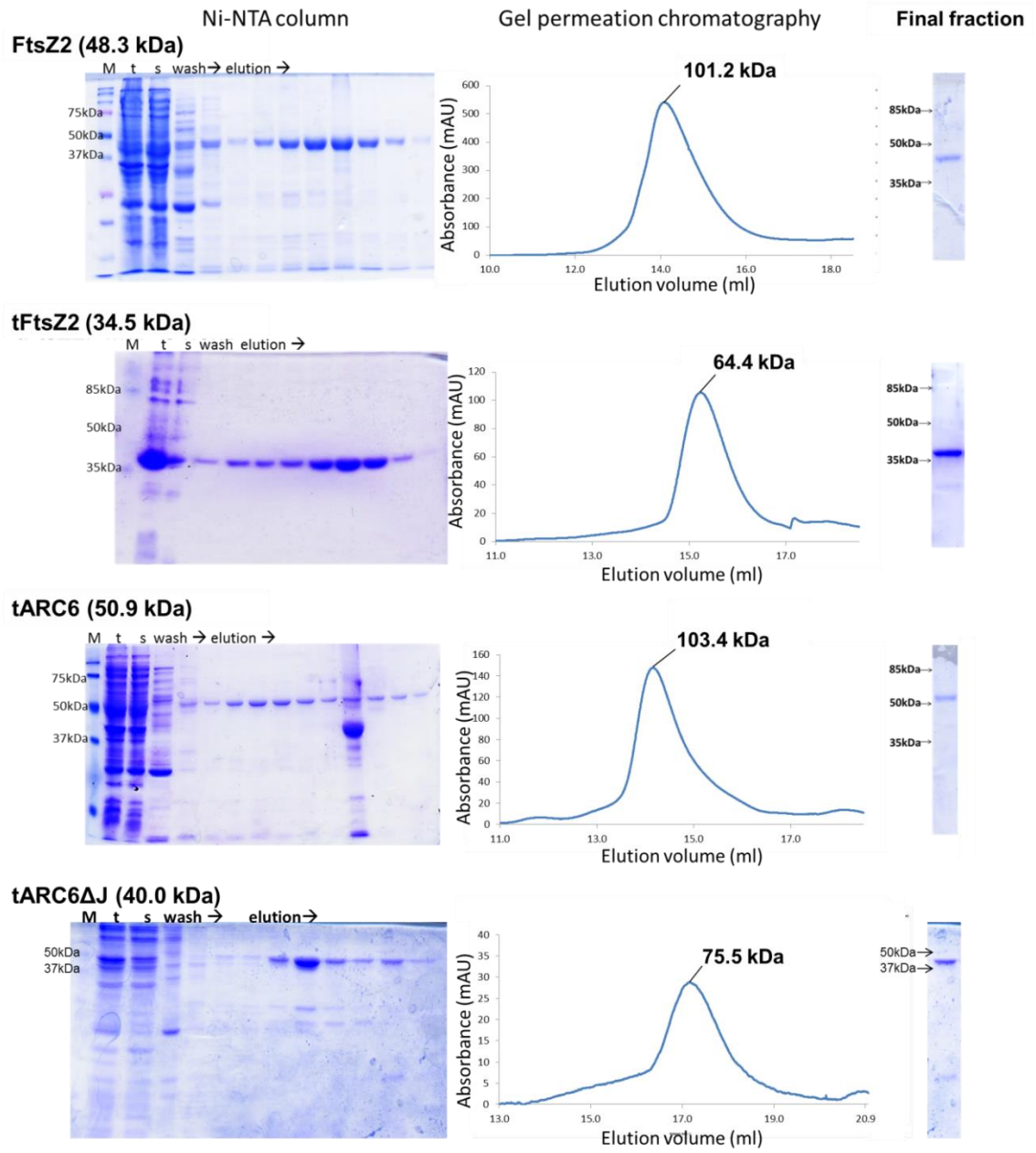

Figure 2-2. Purification of ARC6 and FtsZ2 constructs. Proteins were purified using Ni-NTA column followed by gel permeation chromatography. Fractions from Ni-NTA column were analyzed by 15% SDS-PAGE gel (left panel) and elution profile (middle panel) is shown. Purity of proteins were assessed by densitometry and shown with SDS-PAGE analysis (right panel): 89.1% purity for tFtsZ2 and >98% purity for FtsZ2, tARC6 and tARC6ΔJ. Molecular weight for each protein is indicated. All of proteins were eluted as dimeric size and estimated molecular weights are indicated in chromatographs. M: molecular marker, t: total, s: supernatant.

2.2.3 Effects of ARC6 on the Assembly of FtsZ2 *in vitro*

The effects of ARC6 on FtsZ2 polymerization were assessed by three complementary techniques, namely 90° light scattering, sedimentation, and transmission electron microscopy. Assembly was performed at close to plastid's physiological condition at pH 7.5, 25 C° [72] . FtsZ2 was used at lower concentration (2 μM) in order to provide overall lower rates of assembly where increased FtsZ2 assembly caused by the presence of ARC6 proteins would be easier to monitor.

FtsZ2 assembly was initiated by addition of 1 mM GTP and monitored for 5 minutes by light scattering. FtsZ2 at FtsZ2:tARC6=2:2 molar ratio assembled at approximately 2 fold higher rate compared to FtsZ2 alone. FtsZ:tARC6=2:3 molar ratio yielded a 3-fold increase, confirming that tARC6 acts in a dose-dependent manner to promote FtsZ2 assembly (Figure 2-3, A). When the same assay was conducted with the truncated form FtsZ2 (tFtsZ2) lacking the C-terminal conserved domain, tFtsZ2 assembly was not affected by tARC6 (Figure 2-3, B). This was not surprising since the C-terminus of FtsZ2 is required for interaction with ARC6 [27, 53, 54, 61]. These control experiments confirmed that tARC6 acts solely through interactions with the C-terminal conserved region and also indicated that the light scattering assays in the presence of tARC6 were not influenced by overall elevated protein concentration, i.e., molecular crowding. Effect of ARC6ΔJ on FtsZ2 assembly was also tested and showed increased light scattering in a dose-dependent manner similar to the effect of tARC6 (Figure 2-3, C). The rate of FtsZ2 assembly in reactions with ARC6ΔJ was not significantly different (P=0.05) from rates

in reactions with tARC6 (Figure 2-3, D), indicating that the J-like domain does not play a role in facilitating FtsZ2 assembly *in vitro*.

To further analyze the interaction of FtsZ2 with tARC6, co-sedimentation assays were performed at centrifugation speed where only large filaments may be pelleted with its interacting proteins [67]. Assembly reactions with 2 μM FtsZ2 or tFtsZ2and increasing stoichiometric ratios of tARC6 were centrifuged and separated by SDS-PAGE. The tARC6 co-pelleted with FtsZ2 filaments confirming the interaction between FtsZ2 filaments and tARC6. Fractions of FtsZ2 in the pellet at increasing stoichiometric ratios of tARC6 were elevated in comparison to that when FtsZ2 was assembled alone (Figure 2-3, A) in accord with the results of light scattering assays. This indicated that the presence of tARC6 results in increased abundance or size of FtsZ filaments in a dose-dependent manner. The amount of tARC6 was less than amount of FtsZ2 in the pellet when equimolar amount of FtsZ2 and tARC6 were used, suggesting that ARC6 is not bound to FtsZ2 in the filament at 1:1 molar ratio (Figure 2-3, E).

In control experiments with tFtsZ2, tARC6 did not promote tFtsZ2 sedimentation. A weak tARC6 band was observed in all pellets from tFtsZ2 mixtures, but this was not a result of tFtsZ2-tARC6 interaction, since reactions with tARC6 alone showed a similar band (Figure 2-3, G). Together with light scattering assays of tFtsZ2 assembly in the presence of tARC6 (Figure 2-3, B), these results showed that tFtsZ2 assembly was independent of tARC6 and thus there was no functional interaction between tFtsZ2 filaments and tARC6. FtsZ2 was assembled in the presence of GFP-tagged tARC6 and confirmed its co-localization (Figure 2-4).

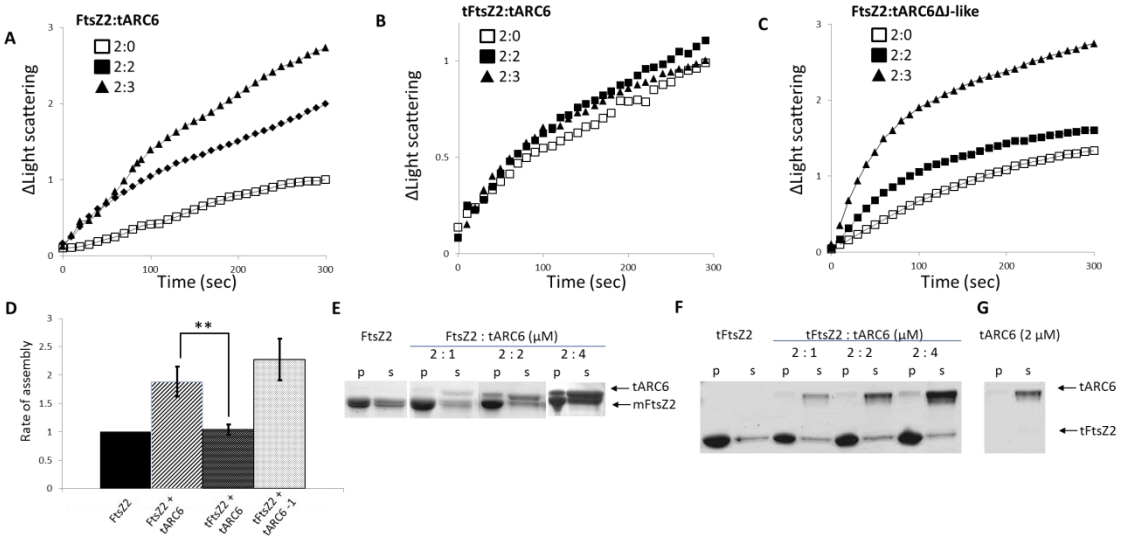

Figure 2-3. tARC6 facilitate FtsZ2 assembly through interaction. Assembly of 2 μM FtsZ2 (A) and 2 μM tFtsZ2 (B) were monitored by 90 degree light scattering at indicated stoichiometric ratio of tARC6 (89-519) respectively. (C) Indicated stoichiometric ratio of tARC6ΔJ-like (157-801) was also used for 2 μM FtsZ2 assembly and monitored by light scattering. Each plot (A-C) is representing repeated assay which had similar light scattering patterns. (D) 2 μM FtsZ2 or tFtsZ2 assembled in the presence of 2 μM tARC6 and 2 μM FtsZ2 in the presence 2 μM tARC6ΔJ-like. The rate of assemblies was measured and plotted for each assembly mixtures as indicated. n=9 and n=5 for assembly mixture of FtsZ2 or tFtsZ2 with tARC6. n=5 for FtsZ2 assembly mixture with tARC6ΔJ-like n=5. **$p < 0.01$ by Student's t-test. 15 % SDS-PGGE gel shows sedimentation of 2 μM FtsZ2 (E) and 2 μM tFtsZ2 (F) and co-pelleting of tARC6 after assembly at increasing stoichiometric ratio as indicated. (G) 2 μM tARC6 alone was shown as control after sedimentation.

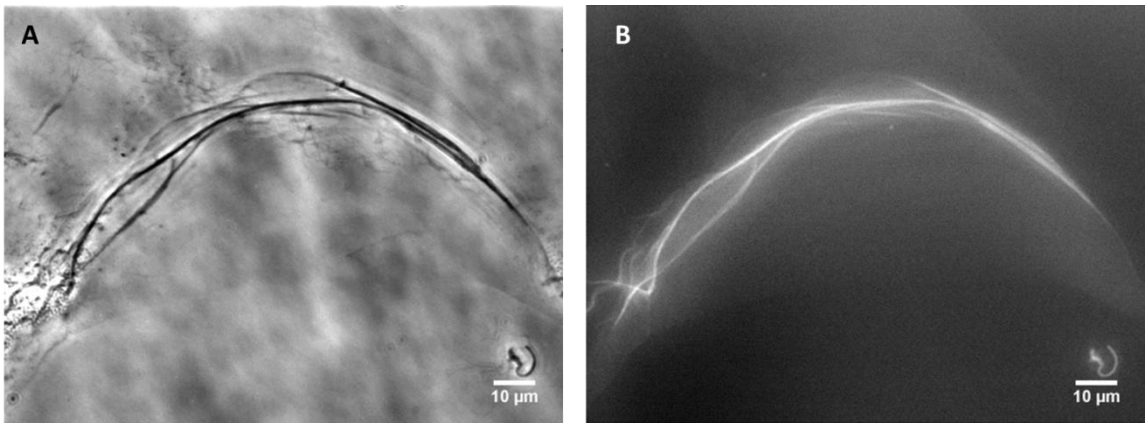

Figure 2-4. Co-localization of GFP-tARC6 on FtsZ2 filaments. (A) FtsZ2 filaments were polymerized in the presence of equimolar amount of GFP-tARC6 and imaged by phase contrast microscopy. (B) Fluorescence signals from GFP-tARC6 were revealed on confocal microscope showing co-localization on FtsZ2 filaments *in vitro*.

Taken together, the data confirms that the conserved N-terminal portion of ARC6 is affecting FtsZ2 assembly *in vitro* by interaction with its C-terminal conserved domain and that membrane tethering is not required for this function. This is consistent with an *in vivo* study of stromal ARC6 [59].

2.2.4 Analysis of FtsZ2 filament bundles using electron microscopy

Light scattering and sedimentation assays demonstrated that tARC6 increases the abundance and/or size of FtsZ assemblies. This effect was not as dramatic as was reported in studies of bacterial FtsZ positive regulators of assembly that promote bundling of FtsZ filaments [64, 73, 74]. To assess FtsZ2 filament morphology and size and to gain insight into how tARC6 promotes FtsZ2 filament assembly, transmission electron microscopy (TEM) was employed. The same assembly reactions used in the

light scattering assays were prepared, negatively stained and examined by TEM (Figure 2-5, A-C).

The images revealed a mixture of FtsZ2 filaments and bundles as well as short protofilaments and non-assembled FtsZ2 subunits (Figure 2-5, A-C). The length and thickness of 1363 and 1501 filaments was measured in FtsZ2 alone and FtsZ2+ tARC6 reactions, respectively (Figure 2-5, D, E). Interestingly, FtsZ2 did not form higher-order or different types of assemblies in the presence of tARC6. This was in contrast with reports on prokaryotic positive regulators of FtsZ assembly such as ZipA and FtsA and other proteins, which induce FtsZ to form cross-linked or bundled filaments by ZapA [75], bundled polymers by ZapD [64], tubules by SepF [76], and curved polymers by FzlA [77, 78]. FtsZ tubules and curved FtsZ polymers are shown for comparison (Figure 2-5, C, bottom panels).

FtsZ2 filament bundles assembled alone were approximately 7 nm thicker than FtsZ2 filaments assembled in the presence of tARC6 (**$p < 0.05$), while their lengths did not differ significantly ($p > 0.05$ by Student's t-test). At higher magnification, FtsZ2 filament bundles assembled in the presence of tARC6 appeared to have somewhat larger gaps between filaments within filament bundles (Figure 2-5, C, upper panels), possibly because of bound tARC6 interfering with tight stacking of filaments in the bundle.

The lack of higher order FtsZ2 structures in the presence of tARC6 suggested that tARC6 does not promote longitudinal or lateral interactions between FtsZ2 filaments and may function through FtsZ2 dynamics, by either increasing assembly rates or decreasing disassembly of assembled filaments. Indeed, the stromal portion of ARC6 was shown to

decrease FtsZ2 subunit turnover in a heterologous expression system [59], suggesting that ARC6 may inhibit disassembly or dissociation of FtsZ subunits in the filament.

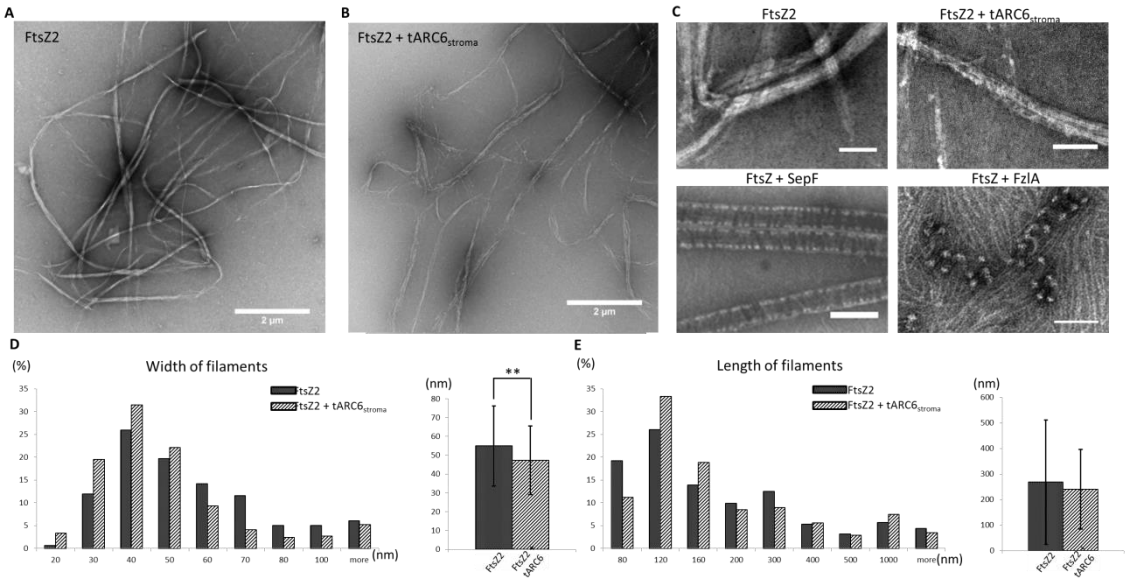

Figure 2-5. Analysis of FtsZ2 filaments using TEM. 2 μM FtsZ2 was assembled in the absence and presence of 2 μM tARC6 and negatively stained and imaged on TEM for analysis. 2 μM FtsZ2 filament bundles in the absence (A) and presence of 2 μM tARC6 (B) were images at x 10K magnification. Scale bar corresponds to 2 μm. (C) In the higher magnification, FtsZ2 filaments were imaged as indicated (upper two panels) to show details. For comparison, bacterial FtsZ filaments with SepF which form tubules [76], and with FzlA which form curved polymers [78] (down two panels) are shown and images were adapted from previous paper [1-2]. Scale bars correspond to 100 nm. Distribution and averages of width (D) and length (E) of FtsZ2 filament bundles in the presence and absence of tARC6 were analyzed and plotted respectively.

To further investigate this hypothesis, non-hydrolyzable GTP analogue GpCpp was used for FtsZ2 assembly in the absence or presence of tARC6. Because FtsZ subunit turnover and filament disassembly require GDP-bound form of FtsZ2, the non-hydrolyzable analogue yields stable FtsZ2 filament that are not prone to diassembly. Low concentration of GpCpp (0.1 mM) was used to maintain a relatively slower assembly rate where the effect of tARC6 could be observed with error range smaller than can be achieved at high assembly rates. The rate of assembly of FtsZ2 was not affected by tARC6 (Figure 2-6,A, B) when GpCpp was used. This indicated that the dynamic assembly and disassembly of FtsZ2 driven by GTP binding and hydrolysis are required to exert tARC6strom effect on FtsZ2. In other words, tARC6 does not promote FtsZ polymerization but rather inhibits disassembly of existing FtsZ2 filaments

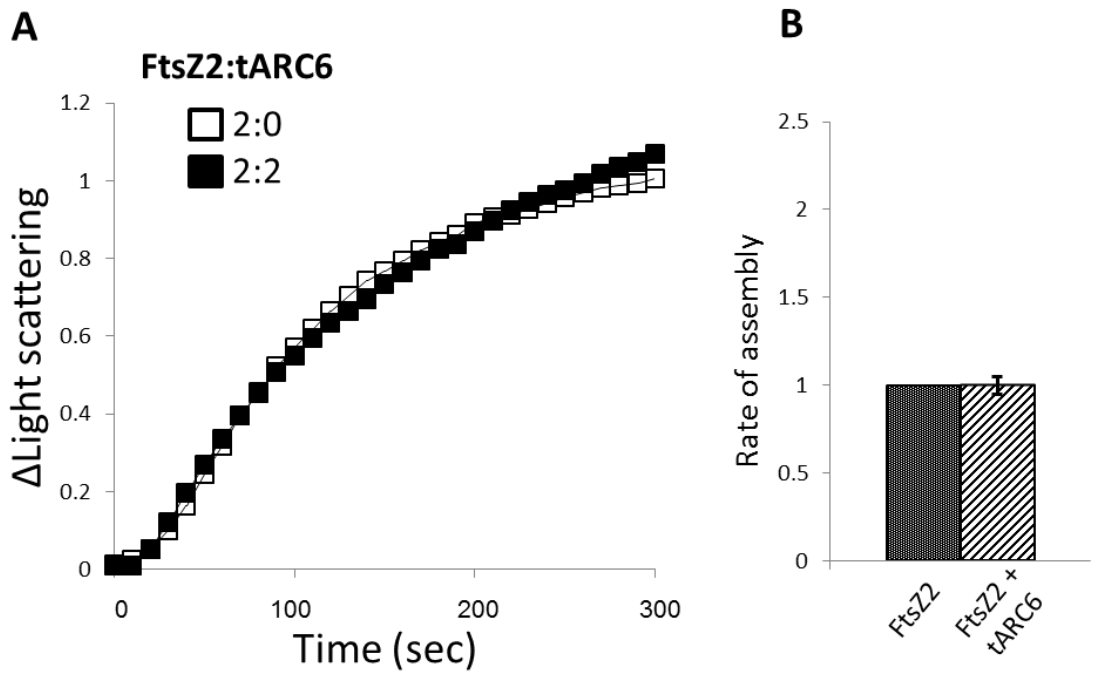

Figure 2-6. FtsZ2 polymerization by Non-hydrolysable GTP analogue GpCpp. (A) 2 μM FtsZ2 in the absence and presence of 2 μM tARC6 were polymerized by addition of 0.1 mM Non-hydrolysable GTP analogue GpCpp and assemblies were monitored by light scattering. The plot is representing repeated assay which had similar light scattering patterns. (B) The rate of assemblies from (A) were measured and plotted. n=6.

2.3 DISCUSSION

2.3.1 Constructs

Full length ARC6 and truncated forms of ARC6 and FtsZ2 were introduced into *E. coli* Rosetta (DE3) pLysS for protein expression. Expression of FtsZ2 and tFtsZ2 significantly inhibited cell division, pointing to functional and structural similarities between the prokaryotic cell and chloroplast division machineries [79]. We have

observed similar effects with other chloroplast division proteins expressed in *E. coli*, such as ARC3, MinD, MinE, as well as ARC6, tARC6 and ARC6ΔJ constructs in this report, probably due to their interactions with the bacterial FtsZ protein, an ancestor of the chloroplast division protein FtsZ2 [7]. The conserved C-terminus of FtsZ2 (463-470) includes F466 which is known as a key residue in interaction with ARC6 [12, 53]. Sequence alignment with the corresponding conserved C-terminus of *E. coli* FtsZ (374-381) shows 62.5 % sequence identity, including the said phenylalanine (Figure 2-7). Expression of ARC6ΔN and ARC6ΔC (Figure 2-1, C) did not disrupt *E. coli* cell division, suggesting that neither fragment is by itself sufficient for interaction with bacterial FtsZ (to disrupt cell division). While it is possible that even after induction with IPTG the expression levels were too low to show an effect, we disfavor this explanation since bacterial cell division is very sensitive to proper balance of division proteins and even small disturbances in their interactions result in observable phenotypes [66, 80, 81].

```
Arabidopsis FtsZ2-1      463 IPEFLKKK 470
Escherichia coli FtsZ    374 IPAFLRKQ 341
                             ** **:*:
```

Figure 2-7. Sequence alignment of conserved C-terminus tail of FtsZ2-1 and *E. coli* FtsZ. Sequence alignment of conserved C-terminal tail of *Arabidopsis* FtsZ2 and *E. coli* FtsZ. Conserved residues are marked with stars and residues with the same charges are marked with colon respectively. (SIM - Alignment tool: http://web.expasy.org/sim)

tARC6 and ARC6ΔJ were previously reported to self-interact in chloroplasts *in vivo* [53]. The presented results of recombinant protein purification and single particle analysis are consistent with this finding and indicate that tARC6, as well as ARC6ΔJ, form dimers *in*

vitro. Dimerization was also observed in our recent work with the full length mature form of ARC6 (data not shown). In contrast, a recent study reported the recombinant N-terminal portion of ARC6 (76-618) to be monomeric and concluded that dimerization of full-length ARC6 is mediated through its c-terminal conserved region via interactions with the PDV2 protein in the intermembrane space of the chloroplast [28]. That study used a buffer containing reducing agents, which may explain the discrepancy – preliminary tests indicated that under reducing conditions, our tARC6 construct also forms a monomer. This brings an interesting possibility that *in vivo*, changes in redox conditions of the chloroplast, e.g. due to changes in light conditions, may play a role in modulating dimerization and possibly activity of ARC6.

2.3.2 Light scattering and TEM

FtsZ2 assembled at higher rate when tARC6 or ARC6ΔJ was present and this effect was dose-dependent (Figure 2-3, A, C). This was not surprising since it was known that the conserved stromal portion of ARC6 interacts with the C-terminus of FtsZ2 [27, 53, 54, 61] and facilitates FtsZ2 assembly [30, 53, 54, 59]. Interestingly, at FtsZ2:tARC6=2:2 stoichiometric the amount of tARC6 co-pelleted with FtsZ2 was less than that of FtsZ2 (Figure 2-3, E), suggesting that the interaction between tARC6 and FtsZ2 filaments is approximately FtsZ2:tARC6=2:1 or less. Furthermore, FtsZ2 and tARC6 did not co-migrate as a complex in gel permeation chromatography (data not shown), suggesting a rather weak or transient interaction between FtsZ2 and tARC6 [59]. Results from assembly of tFtsZ2 in the presence of tARC6 confirmed that the C-terminus of FtsZ2 is

as essential for *in vitro* ARC6-FtsZ interaction as it is in in-vivo experiments [53]. The role of the J-like domain of ARC6 remains unclear. Maple et al.,[53] demonstrated that it not required for FtsZ binding an our data confirmed that it does not alter tARC6 activity towards FtsZ2 assembly or stabilization (Figure 2-3, C,D) .

Unlike bacterial positive regulatory proteins for FtsZ assembly [73-78], ARC6 did not promote formation of higher-order FtsZ2 structures (Figure 2-5, A-E) nor was the increase in light scattering in the presence of tARC6 very dramatic (Figure 2-3, A, D). It is possible that tARC6 may induce FtsZ2 filament nucleation at the initial phase of assembly by stabilizing FtsZ2 dynamics (reducing disassembly rates. And these filaments assemble into bundles without forming higher order structures but more abundant than FtsZ2 filament bundles alone. Furthermore, tARC6 did not exert it effect of more of light scattering during FtsZ2 assembly initiated by addition of non-hydrolyzable GTP analogue GpCpp. This is directly indicating that FtsZ2 dynamics is required to exert the role of tARC6 and suggests promoting longitudinal or lateral interaction by recruiting FtsZ2 units or proto-filaments is not the mode of action for tARC6. Increased FtsZ2 light scattering might be correlated to mass of FtsZ2 polymers rather than the length of filament bundles as far as the length of filament bundles is 3.5 fold longer than the incident wave length [82, 83].

2.4 EXPERIMENTAL PROCEDURES

2.4.1 Cloning of the ARC6, FtsZ1 and FtsZ2 constructs

Full-length mature form of ARC6 (89-801) without the predicted transit peptide (1-67) and a truncated form of ARC6 (89-519) containing the conserved J-like domain and subsequent conserved N-terminus region were cloned into pET28a vector and introduced to *E. coli* Rosetta (DE3) pLysS strain for protein expression. cDNA sequences encoding the mature forms FtsZ2 (49-478) [43] were cloned into pET28a, and *E. coli* Rosetta (DE3) pLysS was used for protein expression. Truncated versions of FtsZ2 (tFtsZ2, 118-424) were designed and expressed in *E. coli* in a similar manner.

2.4.2 Purification of FtsZ2 and ARC6 constructs

2 liters of cells were cultured at 37°C until OD600=0.4 and induced by 0.5mM IPTG. Cells were cultured at 18°C overnight and harvested and lysed by French Press by 20,000 psi in lysis buffer (20 mM Tris-HCl pH 8.0, 500 mM NaCl, 1 mM PMSF). Lysate was centrifuged at 14000 rpm for 1 hour at 4 °C. Proteins were purified by Ni-NTA column, and then further purified by SEC650 gel permeation column (Bio-Rad).

2.4.3 FtsZ2 assembly and disassembly using 90 Degree Light scattering

FtsZ2 (2 μM) in polymerization buffer (50mM HEPES, pH 7.5, 100 mM KCl and 1 mM MgCl2) was polymerized in the absence and presence of 2 μM tARC6 by addition of 1 ul of nucleotides from the stock to the final concentration of 1 mM GTP or 0.1 mM GpCpp. Assembly kinetics was monitored continuously for 5 min by 90° angle light

scattering in a Hitachi fluorometer (Hitachi Model F-4500 FL Spectrophotometer) with both the excitation and emission wavelengths set at 350 nm and a slit width of 5 nm. Polymerization was performed in a thermostatically controlled fluorimeter cuvette at 25 °C by a circulating water bath. Disassembly was performed as previously described [84] with modification. FtsZ2 (2 μM) was polymerized by addition of 0.1 mM GTP at 25 °C in polymerization buffer for 5 minutes as described above. GDP was added to a final concentration of 3 mM to induce the disassembly of FtsZ2 filaments. Light scattering was monitored continuously for 5 minutes as described above. Data was exported into Microsoft Excel for plotting and processing. Rate of assembly or disassembly was estimated by slope where linear increase or decrease of light scattering was observed with correlation coefficient higher than 0.95 at initial phase.

2.4.4 Sedimentation assay

FtsZ2 and ARC6 proteins were pre-centrifuged at 29,700 g for 10 minutes at RT using SIGMA 3-18K Centrifuge and the supernatants were used for the assay. 2 uM FtsZ2 was polymerized in the absence and presenceof 1 uM, 2uM or 3uM tARC6 as previously described above and centrifuged in the same condition. Supernatants were transferred to clean tubes and the pellets were resuspended by 6x sample buffer. The pellet was resuspended in the equivalent volume of polymerization buffer (50mM HEPES, pH 7.5, 100 mM KCl and 1 mM MgCl2) and 6x sample buffer. After boiling the supernatant and pellet, 20 ul of samples were loaded on 15% SDS-PAGE gel. The gel was stained by Coomassie Brilliant Blue G-250.

2.4.5 Electron microscopy and image analysis

Assembly mixtures from the light scattering were used for negative stain and electron microscopy. Carbon-coated Formvar grids were freshly glow-discharged and 5 μL of the reaction mixtures were adsorbed for approximately 10 seconds, washed briefly in water, and negatively stained with a 2% (w/v) aqueous solution of uranyl acetate (pH 4.5). Specimens were observed in a JEOL 1200 EX transmission electron microscope operated at an acceleration voltage of 100 kV. Electron micrographs were recorded at calibrated magnifications using a 3k slow-scan CCD camera (model 15C, SIA).

CHAPTER III

STABILIZATION MECHANISM OF FTSZ2 FILAMENTS BY ARC6

3.1 INTRODUCTION

Our data showed that stromal portion of ARC6 facilitate FtsZ2 assembly without forming higher order structures *in vitro*. Previously fluorescence protein tagged stromal portion of ARC6 was co-expressed with FtsZ2 in heterologous expression system and showed significantly reduced turnover of FtsZ2 [59] which provides clues for possible the mode of action for ARC6. However, the biochemical characterization of the effect of ARC6 on FtsZ2 assembly is still not fully defined *in vitro* up to date. Previously, ARC6 was suggested to perform an analogue role as bacterial cell division proteins ZipA and FtsA [53] and possible mechanical roles of ARC6 for FtsZ assembly can be guided by these functional homologues.

FtsA is known to tether Z-ring to membrane through direct interaction with C-terminal tail of FtsZ and co-localize with FtsZ filament [73, 85, 86]. And the intercellular ratio of FtsZ and FtsA *in vivo* for their function is estimated approximately 5:1 in both *E. coli* and *Bacillus subtilis* (*B. subtilis*) [65, 66] suggesting that ARC6 may function at a specific stoichiometry. Effects of FtsA have been revealed as a dual, antagonistic role of FtsA: recruitment of FtsZ filaments to the membrane and negative regulation of FtsZ polymerization [73, 87]. Previous studies showed that FtsA from *Deinococcus radiodurans* stimulates GTPase activity of its FtsZ while FtsZ from *E. coli* was affected

negatively [88], and FtsA from *Staphylococcus aureus* increased GTPase activity of its FtsZ [89] although this is not directly related to promoting FtsZ assembly [88, 89]. ZipA is known to promote bundling of FtsZ filaments *in vitro* [90, 91] via interaction with C-terminus of FtsZ with C-terminus of FtsA [91, 92]. ZipA stabilized FtsZ polymers against dilution induced disassembly [74] and localize FtsZ filaments to the membrane without affecting GTPase activity or dynamics of the FtsZ filaments [92-94]. It was previously suggested that N-terminal portion of ARC6 may retain the function as bacterial protein for plastid division, while C-terminal portion of had evolved for new chloroplast-specific protein–protein interactions such ARC6-PDV2 interaction to coordinate recruitment of division machinery components located on the cytosolic side of the chloroplast [1]. However, our studies have shown that stromal portion of ARC6 facilitate FtsZ2 assembly without promoting bundles. In addition, it is known that dynamics of FtsZ2 is affected by ARC6 [59] unlike bacterial ZipA suggesting that ARC6 may have evolved to invoke a different mode of action.

Whether stromal portion of ARC6 affects GTPase activity of FtsZ2 and how ARC6 reduced turnover of FtsZ2 are not known. To investigate the mechanistic role of stromal portion of ARC6, GTPase activity of FtsZ2 was measured in the absence and presence of ARC6. Also, to test the possibility that ARC6 works through dynamics of FtsZ2 to facilitate the assembly, GDP was added to the assembly mixtures since it known that GTP hydrolysis by FtsZ is generally correlated with dynamics of FtsZ [46, 95].

Our results showed that stromal portion of ARC6 stabilized FtsZ2 filaments in the GDP-induced disassembly condition and has significant effect on FtsZ2 assembly initiated by

non-hydrolyzable GTP analogue GpCpp when excess amount of GDP is present. These results suggest that tARC6 prevents immediate disassembly and thereby facilitate FtsZ2 assembly.

3.2 RESULTS

3.2.1 FtsZ2 and FtsZ2D322A assembly and dynamics when expressed alone and with tARC6 in *S. pombe*

A previous FRAP study has shown that *in vivo*, FtsZ2 filaments become stabilized in the presence of stromal portion of ARC6 and subunit turnover is inhibited [59]. Also, GTPase-deficient FtsZ2 D322A had significantly reduced turnover, confirming that GTP hydrolysis is an important factor in filament dynamics [43]. To expand this analysis, we expressed the *Arabidopsis* FtsZ2 and FtsZ2D322A GTPase-deficient mutant alone or coexpressed with tARC6 in the fission yeast *S. pombe* to assess their inherent assembly and dynamics characteristics and to establish how tARC6 affects them. Consistent with previous reports [43, 59] tARC6 expressed well and adopted a diffuse localization pattern (Figure 3-1, A), while FtsZ2 and FtsZ2D322A assembled a network of interconnected filaments and aster-shaped structures, respectively (Figure 3-1, B-C). Coexpression of tARC6 and FtsZ2 resulted in the proteins colocalizing to an interconnected network of filaments (Figure 3-1, C), which were highly similar to that assembled by FtsZ2 alone. Pearson's Correlation Coefficients was used to estimate the extent of fluorescence signal overlap and the degree to which the fluorescent signal intensities were correlated. FtsZ2 and tARC6 had a PCC of 0.92 ± 0.01 (± SEM, n = 10),

suggesting that these proteins were highly colocalized into the filament network. Similarly, FtsZ2D322A and tARC6 colocalized to FtsZ2D322A-like structures when coexpressed. However, tARC6 had a more diffuse signal in this coexpression strain than when coexpressed with FtsZ2, with a PCC of 0.81 ± 0.03 (± SEM, n = 10), a statistically significant reduction compared to tARC6 coexpressed with FtsZ2 (P-value = 0.0004), suggesting that tARC6's interaction with FtsZ2D322A is weaker than that of FtsZ2. The steady-state turnover properties of these filamentous structures were analyzed using fluorescence recovery after photobleaching (FRAP) (Figure 3-1, F-G). The time-course fluorescence recovery curves fit a two-binding state equation that yielded the fractions of bound molecules (c_{eq1} and c_{eq2}) and their respective unbinding rate constants (k_{off1} and k_{off2}, s-1). All results are summarized in table I. When expressed alone, FtsZ2 fluorescence signal recovered to 29% of the initial intensity after 250 s with an initial recovery rate of 5.1e-3 normalized fluorescence units/s (NFU/s). When coexpressed with tARC6, FtsZ2 showed similar dynamic parameters with slightly lower initial rates of recovery (Table 1). tARC6 had initial recovery rate of 7.0e-3 NFU/s and recovered to 76% of the initial fluorescence. FtsZ2D322A showed nearly no recovery: initial recovery rate of 1.4e-3 NFU/s, recovering to only 8% of the prebleach fluorescence intensity, and with greatly reduced unbinding rates than those of FtsZ2. When coexpressed with tARC6, FtsZ2D322A also showed nearly no fluorescence recovery. However, tARC6 showed a substantial increase in initial rate of fluorescence recovery and the extent of recovery at 250 s, indicating that tARC6 binds FtsZ2D322A less tightly than FtsZ2.

Table 1: FRAP data for all single and coexpression strains

Protein	r	c_{eq1}	c_{eq2}	k_{off1}	k_{off2}	Recovery Slope	Recovery @ 250 s	n
FtsZ2-eCFP	0.2100	0.8637	0.1351	1.2411e-3	0.1109	5.1e-3	29%	11
FtsZ2-eCFP + $ARC6_{stromal}$-mVenus	0.4960	0.8312	0.1668	3.6870e-3	6.6514e-2	4.7e-3	34%	10
	0.1867	0.9566	4.0723e-2	1.0773e-2	0.4063	7.0e-3	76%	11
FtsZ2D322A-eCFP	-56.6495	0.9991	7.7875e-4	1.6252e-6	2.5578e-2	1.4e-3	8%	10
FtsZ2D322A-eCFP + $ARC6_{stromal}$-mVenus	-3.5712	0.9919	8.0789e-3	3.2587e-5	0.1700	1.9e-3	7%	12
	6.9578e-2	0.4203	0.5794	1.3683e-2	0.1254	2.93e-2	92%	10

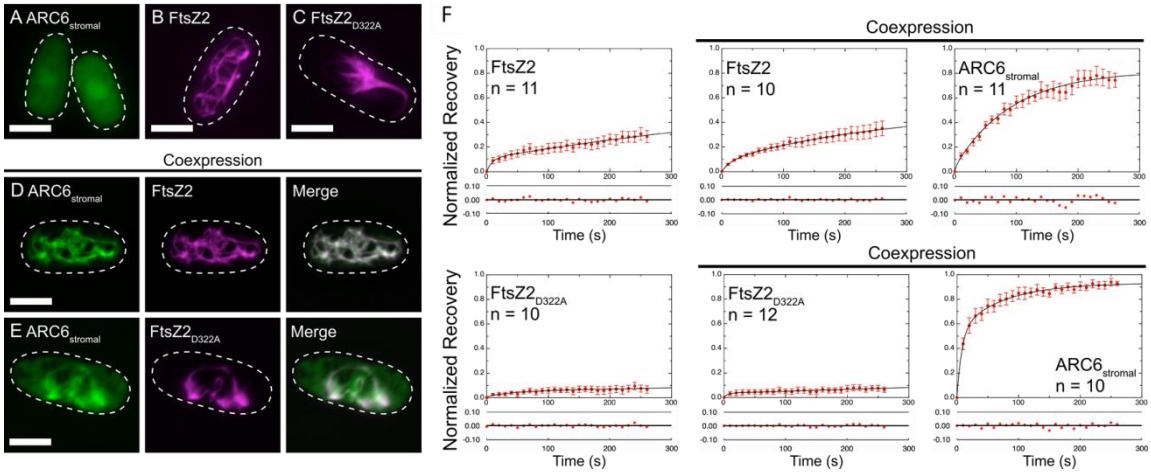

Figure 3-1. Filament assembly and subunit exchange characterization in *S. pombe*. (A-E) Epifluorescence micrographs of (A) ARC6stromal-mVenus, (B) FtsZ2-eCFP, (C) FtsZ2D322A-eCFP, (D) ARC6stromal-mVenus coexpressed with FtsZ2-eCFP, and (E) ARC6stromal-mVenus coexpressed with FtsZ2D322A-eCFP. Fluorescent signals from ARC6stromal-mVenus are falsely colored green, while those of FtsZ2-eCFP and FtsZ2D322A-eCFP are falsely colored magenta. The white color in merged images represents regions where the two fluorescence signals overlap and colocalize. Dashed lines represent cell outlines. Bars, 5 μm. (F-G) FRAP analysis of FtsZ2-eCFP and FtsZ2D322A-eCFP expressed alone and with ARC6stromal-mVenus. (F) Graphs (top) of the Normalized fluorescence recovery vs time (s) for all *S. pombe* single and co-expression strains. Graphs (bottom) show that all data points are well within 0.10 normalized recovery units (10%) from the fitted curve. The data are normalized to the pre-bleach fluorescence intensity (1 on the y-axis) and the fluorescence intensity at the time of photobleaching (0 on the y-axis). n represents the number of independent FRAP experiments performed. Error bars represent SEM at each time point.

3.2.2 ARC6 stabilizes FtsZ2 filaments and slows down GDP-induced disassembly

Slower turnover of FtsZ2 filaments by tARC6 in prior [59] and current FRAP experiments suggested that FtsZ is stabilized by tARC6, and therefore less prone to disassembly. To explore this further, FtsZ2 polymerization *in vitro* was initiated by addition of 0.1 mM GTP and after 5 minutes excess GDP - to a final concentration of 3 mM- was added to induce disassembly [47, 84].

Without tARC6, the addition of excess amount of GDP lead to FtsZ depolymerization as judged by decrease in light scattering (Figure 3-2, A). This decrease was substantially slower than what was previously reported for bacterial FtsZ GDP-induced disassembly [47, 84], pointing to overall slower dynamics of plant FtsZ2 in comparison to its prokaryotic homologues. The presence tARC6 resulted in approximately two fold slower disassembly of FtsZ2 filaments (Figure 3-2, B). When the samples were examined by TEM, the large FtsZ filament bundles typically observed in FtsZ assembly reactions (Figure 2-, A, B) were absent after GDP-induced disassembly reactions, regardless whether tARC6 was present or not (Figure 3-2, C-D). However, in the presence of tARC6, FtsZ2 was able to maintain some smaller and thinner filament bundles (Figure 3-2, D) while only short protofilaments remained in the absence of tARC6 (Figure 3-2, C).

The dominant morphology of FtsZ2 filaments remaining after disassembly in the presence of tARC6 (Figure 3-2, D) was characterized as short and curved filament bundles. Curved filaments were previously reported with GDP- bound subunits of prokaryotic FtsZ [96]. It is conceivable that the curved assemblies shown in Figure 3-2,

D represent GDP bound FtsZ2, and that the role of tARC6 is to stabilize FtsiZ2 filaments when GDP-bound FtsZ2 is present.

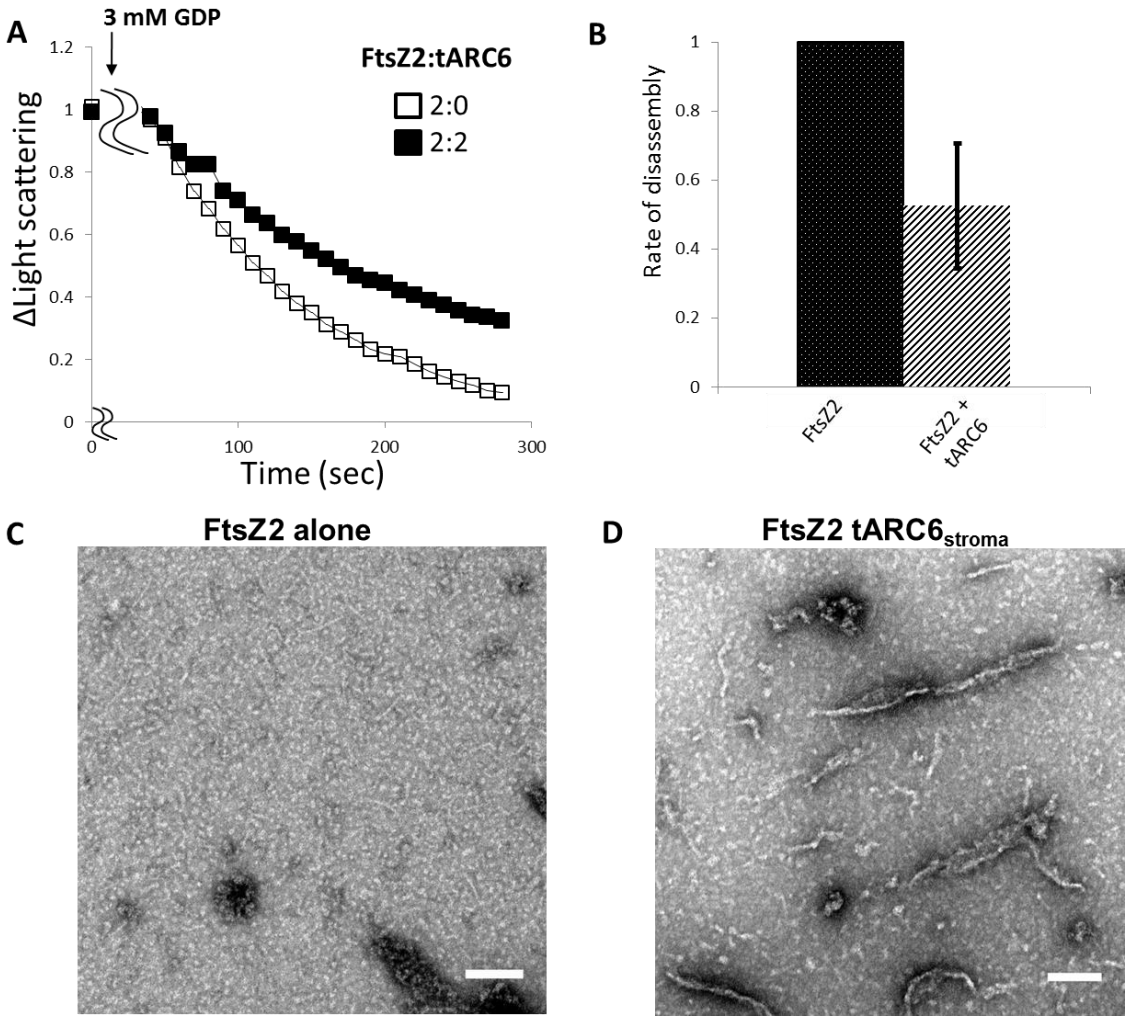

Figure 3-2. Role of ARC6 in stabilizing FtsZ2 filament bundles in disassembly condition. To monitor the rate of disassembly, (A) FtsZ2 was assembled by addition of 0.1 mM GTP and incubated for 5 min and 3 mM GDP was added to initiate disassembly in the presence and absence of 2 μM tARC6 as indicated. (B) the rate of disassembly of FtsZ2 in the presence of equimolar tARC6 was approximately 2 fold slower than the rate of disassembly of FtsZ2. n=5. Samples from both of FtsZ2 polymers from (A) after 10 min of disassembly was taken and negatively stained for TEM images. Short and thin FtsZ2 filament bundles were present in the presence of tARC6 (D) while only short FtsZ2 protofilaments were remained in the absence of tARC6 (C).

3.2.3 Mechanical role of tARC6 on FtsZ2 filament stabilization

To further investigate the role of tARC6, two possible roles where tARC6 could modulate FtsZ2 dynamics to stabilize FtsZ2 filaments were tested.

Firstly, tARC6 may affect assembly by modulating GTPase activity of FtsZ2. It is reported that FtsA proteins from *Deinococcus radiodurans* and *Staphylococcus aureus* stimulate GTPase activity of their FtsZ proteins respectively although this is not directly related to promoting FtsZ assembly [88, 89]. Increased GTP binding and hydrolysis by FtsZ proteins eventually lead to depolymerization of filaments [88, 97]. Thus, tARC6 could reduce or inhibit GTPase activity of FtsZ2, rendering the FtsZ2 polymers less prone to disassembly and less dynamic. To test this possibility, GTPase activity of FtsZ2 was measured in the absence or presence of equimolar amount of tARC6 (Figure 3-4, A). Overall, GTPase activity of FtsZ2 was not reduced by ARC6 but was rather slightly elevated when tARC6 was present.

Another possibility is that tARC6 could stabilize FtsZ2 filaments by preventing dissociation of FtsZ2 subunits after GTP to GDP hydrolysis. The ratio of GTP to GDP is known as a critical factor for FtsZ filaments [98] because GDP could trigger disassembly allowing filament dynamics [97]. Since tARC6 did not have any effect when GpCpp alone was used in FtsZ2 assembly reactions, a mixture of 0.1 mM GpCpp and 0.2 mM GDP was used to produce assemblies containing predominatly GDP-bound FtsZ2 that are more prone to FtsZ2 subunit dissociation and filament disassembly. In concert with our previous results discussed above, when only 0.1 mM GpCpp was used for FtsZ2

assembly, no significant effect of ARC6 was detected (Figure 3-4, B). In reactions with GpCpp + GDP, light scattering developed at a much lower rate with FtsZ2 alone, indicating that the balance has been tipped towards accelerated disassembly of filaments. (Figure 3-4, B). Strikingly, the presence of tARC6 largely compensated for this effect and produced approximately 3- fold increase in net assembly rates compared to FtsZ2-alone reactions (Figure 3-4, C).

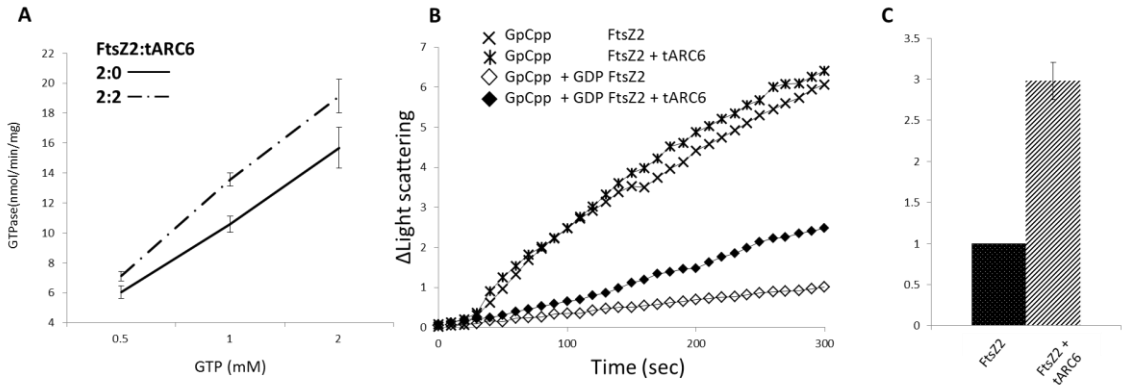

Figure 3-3. Effect of ARC6 on GTPase activity of FtsZ2 and polymerization of FtsZ2 by GpCpp + GDP. (A) GTPase activities of FtsZ2 were estimated at RT after 5 min incubation with addition of 0.5 mM, 1 mM and 2 mM GTP in the presence or absence of equimolar amount of ARC6. (B) Light scattering of 2 μM FtsZ2 polymerization at 0.1 mM GpCpp, 0.1 mM GpCpp mixed with 0.2 mM GDP in the presence and absence of 2 μM ARC6. (C) the rate of 2 μM FtsZ2 assembly in the presence of 2 μM tARC6 with 0.1 mM GpCpp and 0.2 mM GDP was plotted. n=7.

Taken together, these results strongly suggest that tARC6 exerts its effect through GDP-induced FtsZ2 dynamics within filament bundles by preventing immediate dissociation of GDP-bound FtsZ2 subunits, and thereby promoting net FtsZ2 assembly.

3.3 DISCUSSION

3.3.1 ARC6 and the turnover of FtsZ2

Terbush et al., [59] showed in FRAP assays that tARC6 significantly decreased the rate of FtsZ2 polymer turnover in *S. pombe* expression system. The current FRAP data now demonstrated that when coassembled with the GTPase-deficient mutant FtsZ2D322A that forms very stable filaments with minimal turnover, tARC6 exhibited drastically increased subunit exchange kinetics. We interpret these results as an indication that tARC6-FtsZ2 interaction is transient and that tARC6 has low affinity to GTP-bound FtsZ (Figure 3-1, F and Table 1). This was also demonstrated in the light scattering experiments where FtsZ2 assembly was not affected by tARC6 when the assembly was induced by addition of the non-hydrolysable GTP analogue GpCpp (Figure 2-6). Together, FRAP analysis of GTPase deficient FtsZ2D322A confirmed our hypothesis that tARC6 works through FtsZ2 dynamics. The FRAP data provided the best fit with a two binding-state model, showing two populations of tARC6 with different unbinding constants: one fraction of tARC6 has weak interactions with immobile fraction of FtsZ2 polymer while another fraction of tARC6 binds more tightly with the mobile fraction of FtsZ2 polymers, stabilizing them.

3.3.2 GDP induced disassembly

The question that remained was how does tARC6 sabilize FtsZ2 filaments and modulate slower FtsZ2 turnover. Experiment with GDP-induced disassembly of FtsZ2 filaments clearly showed that after addition of excess GDP, equlibrium between assembly and

disassembly of FtsZ2 filaments was shifted significantly toward depolymerization (Figure 3-2, A), but the presence of tARC6 rendered FtsZ filaments to be more resistant to such disassembly and produced curved and twisted morphology of FtsZ2 filaments. Their morphology was similar to longitudinally bent and curved protofilaments of GDP-bound *Mycobacterium tuberculosis* FtsZ [40] and to helically curved GDP-bound FtsZ filaments in *Methanococcus jannaschhi* [97]. Our data are consistent with a model where tARC6 interacts with GDP-containing FtsZ2 filaments and filament bundles and prevents dissociation of GDP-bound FtsZ2 from the filaments.

3.3.3 GTPase activity and GDP/GpCpp

GTPase activity of FtsZ is generally correlated with the rate of assembly and FtsZ subunit turnover in and out of the filament [46, 95] . For FtsZ2 the measured activity was 10.6 ± 1.1 nmol GTP hydrolyzed/min/mg protein when 1 mM GTP was used, a result very close to a previously reported value of 12 ± 0.5 nmol GTP hydrolyzed/min/mg protein) [99] confirming the validity of the GTPase assay.

The GTPase activity of FtsZ leads to depolymerization of filaments eventually [88, 97]. The slightly increased GTPase activity of FtsZ2 in the presence of tARC6 (Figure 3-4, A) was consistent with increased net assembly in light scattering (Figure 2-3, A) but in sharp contrast to the decrease of FtsZ2 turnover in FRAP assays ([59] and Figure 3-1, F). This is suggested that tARC6 does not facilitate FtsZ2 assembly by modulating GTPase activity. The elevated GTPase activity measured in the assays may be simply due to the

fact that in the presence of tARC6 there are more FtsZ2 assemblies and thus the capacity to hydrolyze GTP within filament bundles is increased.

3.4 EXPERIMENTAL PROCEDURES

3.4.1 GTPase activity

GTPase activity was measured using BIOMOL® GREEN Reagent at 25 °C with 50 µL reaction volumes (2 µM FtsZ) in a 96-well flat bottom plate (Falcon). Absorbances at 620 nm were monitored using a Variokan LUX multimode microplate Reader (Thermo Fisher science). Data were plotted using Microsoft Excel and corrected against a sample containing no protein. Background from the buffer and proteins were also measured and subtracted from the GTPase reactions of FtsZ2 in the absence or presence ARC6. GTPase activities given are derived from triplicate experiments.

3.4.2 FRAP *in vivo* from *S. pombe*

3.4.2.1 Construct Generation and Transformation into *S. pombe*

FtsZ2-eCFP and FtsZ2D322A-eCFP constructs were those described in TerBush and Osteryoung [43] and ARC6stromal-mVenus was that described in TerBush et al. [59]. FtsZ constructs were transformed into *S. pombe* using a lithium acetate procedure (http://www-bcf.usc.edu/~forsburg/tfmn.html). *S.pombe* (strain MBY192 [h- leu1-32 ura4-D18]) cultures were grown in 50 mL of yeast extract plus supplements media (YES, http://www-bcf.usc.edu/~forsburg/media.html) for ~40 hours at 32°C. 5x108 cells (50 mL at OD600 = 0.5) were harvested by centrifugation at 4,000g for 10 minutes at room

temp. The resulting cell pellet was washed in 25 mL of TE (10 mM Tris-HCl, 1 mM EDTA, pH 7.5). The cells were pelleted again at 4,000g for 10 minutes at room temp. The cells were resuspended in 1 mL of TE and LiAc (100 mM lithium acetate, pH 7.5) and allowed to incubate at 30°C for 30 min. 200 µL of cells were aliquoted to a 2.0 mL microfuge tube that contained 20 µL of 10 µg/µL carrier sperm DNA (Agilent Technologies) and 1 µg of plasmid DNA (~2-3 µL in 2 mM Tris-HCl, pH 8.5) that had been incubating on ice. Cells were mixed by vortexing. For strains coexpressing 2 FtsZs from separate plasmids, 1 µg of each plasmid DNA was added to the transformation reaction to co-transform both plasmids into *S. pombe* at the same time. 1.2 mL of PEG solution (40% PEG, TE pH 7.5, and LiAc) was added to each tube and vortexed for 10 s. The tubes were incubated at 30°C for 30 min with shaking at 250 rpm. DMSO was added to 5% total volume (71 µL), the cells were vortexed again for 10 s, and then the tubes were incubated at 42°C for 15 min. The cells were pelleted at 7,000g for 30 s, and the supernatant was pipetted off. The cells were resuspended in 300 µL of TE and plated onto solid PMG with selection for each plasmid (-leucine for pREP41 and pREP41X, -uracil for pREP42X, or -leucine/-uracil for strains with both pREP41X and pREP42X) and 15 µM thiamine to repress protein expression [100]. The plates were allowed to grow at 32°C until colonies formed.

3.4.2.2 Growth and Expression of Transformed Cell Lines

Yeast strains containing the FtsZ fluorescent fusions described above were streaked for isolation on solid PMG with 15 µM thiamine, to repress expression. The

plates also lacked leucine, uracil, or both to select for constructs pREP41/pREP41X, pREP42X, or both pREP41X and pREP42X, respectively. Plates were incubated at 30-32°C until colonies formed. Individual colonies were picked and used to inoculate 3 mL of liquid culture without thiamine to induce expression of the fusion proteins. These cultures were allowed to grow at 32°C with 250 rpm shaking for ~40 h to reach steady state conditions for filament assembly and turnover.

3.4.2.3 Fluorescence Microscopy and FRAP Analysis

S. pombe cells grown in liquid PMG media under selection, as described above, were imaged by differential interference contrast (DIC) and epifluorescence microscopy, using a microscope (model DMRA2; Leica, Wetzlar, Germany) with an HCX PL FLUOTAR 100X (1.30 NA) oil-immersion objective (Leica) and a CCD camera (retiga Exi; QImaging, Burnaby, BC, Canada). 2 μL of liquid culture was pipetted onto a glass poly-lysine coated slide and covered with a No. 1.5 coverslip. All imaging was performed at room temperature. Z stacks were taken with 0.5 μm increments. Images were acquired and subsequently de-blurred using nearest neighbor deconvolution at 70% haze removal using Image-Pro 7.0 software (Media Cybernetics). Additional image processing and analysis for epifluorescence micrographs was performed using Fiji software (ImageJ; http://fiji.sc/Fiji). Single-plane projections were generated from Z stacks using the maximum intensity algorithm and were falsely colored magenta for FtsZ2 signals. Coexpression overlays were created with the merge channel tool, where colocalized fluorescence signals appear in white. Colocalization of fluorescence signals

in coexpressing strains was quantified by creating a composite image of the 2 fluorescence signals from a deconvoluted Z stack, cropping the image to contain only the single cell being analyzed, unmerging the 2 channels, using the Coloc2 plugin within Fiji to calculate a Pearson's Correlation Coefficient (PCC) [101], and averaging all PCC values for each coexpression strain, ± SEM.

Fluorescence Recovery After Photobleaching (FRAP) experiments were performed at room temperature on a laser-scanning confocal microscope (Fluoview 1,000 Spectral, Olympus) with a Plan FLN 60X (1.42 NA) oil-immersion objective with a 3.2X zoom. Just prior to performing each FRAP experiment, the high voltage setting for the photomultiplier tube was set so the greatest fluorescence signal in the image was just below saturation. FRAP data were collected with FV1000 ASW software (Olympus). 2 μL of liquid culture was pipetted onto a glass poly-lysine coated slide and covered with a No. 1.5 coverslip. All filaments were bleached for 20 ms at a % laser intensity so that one-half to two-thirds of the fluorescence signal was bleached, and continuous imaging was performed at the minimal laser intensity to minimize photobleaching but still provide adequate fluorescence signal. mVenus and eCFP fusion constructs were imaged and bleached with a 515 and 458 nm laser, respectively. All time-course imaging for FRAP experiments were performed with 10 s intervals between time points. Three images were acquired before bleaching to calculate the average pre-bleach fluorescence intensity, and post-photobleach imaging occurred for an additional 260 s. Fluorescence intensity measurements were acquired for the region of photobleaching, a background sample, and an area of fluorescence signal that was away from the bleach region. Raw

FRAP data was processed to produce photobleaching corrected and normalized recovery datasets (Rabut and Ellenberg, 2005). All datasets for each fluorescent fusion were averaged together to produce the average recovery dataset. Additionally, standard error of the mean (SEM) was calculated for normalized recovery at each time point. This average FRAP recovery dataset was used for curve-fitting using pro Fit software (QuantumSoft), where the data were fit to the two binding states equation from the FRAPAnalyser software (http://actinsim.uni.lu/eng/Downloads): $f(t) = (1 - r)(1 - c_{eq1}*e\text{-}k_{off1}*t - c_{eq2}*e\text{-}k_{off2}*t)$. Initial rates of recovery were calculated from the slope of the initial linear region of recovering fluorescence data points measured during timecourse imaging.

CHAPTER IV

STRUCTURAL CHARACTERIZATION OF ARC6 BY SINGLE PARTICLE ANALYSIS

4.1 INTRODUCTION

Our data have shown that tARC6 eluted as a dimer using gel permeation chromatography (Figure2-2). This is consistent with previous results from yeast-two hybrid experiments showing that the stromal domain of ARC6(1-614) interacts with itself [53]. However, a structural characterization of full length ARC6 in complex with FtsZ2 and PDV2 remains elusive.

The N-terminal portion of ARC6 include two regions: J-like domain (D89-153), which is predicted to be comprised of helixes as DNA-J domain (Figure 4-1, left), and conserved N-terminal region of ARC6 (D89-A519). The first 107 residues (84-290) is known to have interaction with J-like domain of Chloroplast J-like domain 1(CJD1) which influences fatty acid composition of Chloroplast lipids in *Arabidopsis* [63]. The transmembrane domain of ARC6 (619-638) can be integrated into inner envelope membrane (IEM) via its predicted single helix. This single helix has length of approximately 30 Å which is in good agreement with the thickness of lipid bilayer in thylakoid which varies in between 30 Å to 40 Å depends on the lipid type [102] (Figure 4-1, middle). A recent study of stromal portion of recombinant ARC6 to be monomeric and its dimerization is induced by PDV2 via the C-terminal domain of ARC6 located in the intermembrane space [28]. The crystal structure of dimeric C-terminal domain of

ARC6 (green) complexed with C-terminal peptide of PDV2 (red) is shown (Figure 4-1, Right).

In order to reveal the structural and functional relationship of dimeric tARC6, single particle analysis and 3D reconstruction was performed using TEM images of negatively stained monodispersed protein. Here, we represent a three-dimensional reconstruction of tARC6 aimed at an understanding of the possible interaction of the membrane-associated full length ARC6 dimer with the FtsZ2 filament in coordination with PDV2 residing in the outer membrane of the chloroplast envelope.

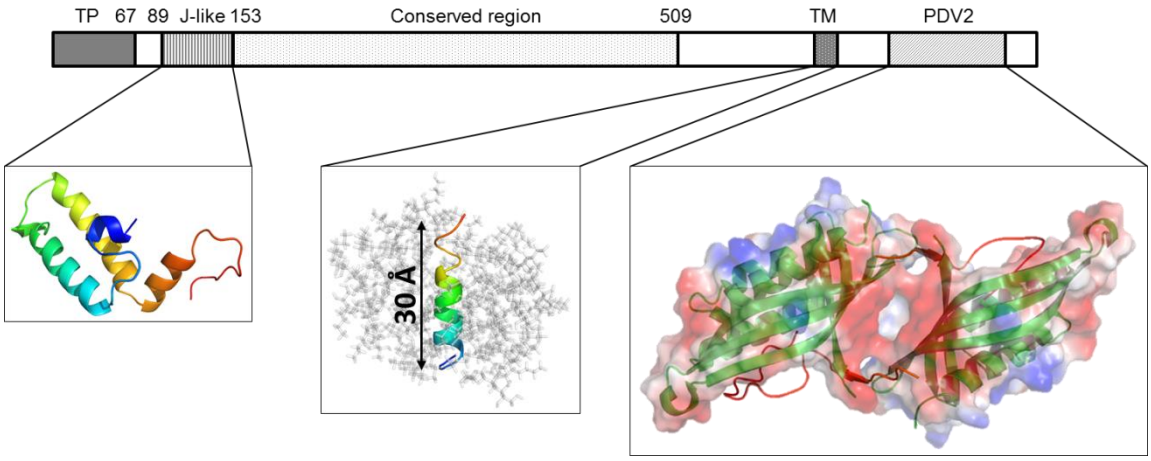

Figure 4-1. Crystal structure of dimerized C-terminal domain of ARC6 and models of J-like domain and transmembrane of ARC6. (A) Full length ARC6 (ARC6) as shown in Figure 2-1. A TP: transit peptide (1-69), J-like: J-like domain (89-153), CR: conserved region (89-509), TM: transmembrane, PDV2:PDV2 binding domain (679-774). (B) Model of J-like domain of ARC6 (89-153) generated based on J-domain of human DnaJ homolog (PDB: 2DN9) using Phyre2 [103]. (C) Model of the transmembrane domain embedded in detergent (1, 2, 3-heptanetriol). Generation of the transmembrane domain model (single helix) and stimulation with 1, 2, 3-heptandtriol has been performed by Dr. Lisa Perez's lab (unpublished data). (D) Top view of the crystal structure of dimeric C-terminal domain of ARC6 (green) complexed with C-terminal peptide of PDV2 (red) (PDB ID:1GTB). Surface potential of C-terminal domain of ARC6 is represented with red for negatively charged residues and blue for positively charged residues.

4.2 RESULTS

4.2.1 3D reconstruction of tARC6 and a model for FtsZ2 binding

For structural characterization of dimeric tARC6, 3D reconstruction was performed to elucidate dimeric status and evaluate the interaction mode with FtsZ2 protofilament. In order to reveal the structural and functional relationship of dimeric tARC6, 3D reconstruction was performed using TEM images of negatively stained monodispersed protein. The reconstruction appeared as horse shoe- like dimeric form at near 2 nm resolution (Figure 4-2, E). The width and length of the reconstruction were

approximately 7 nm and 8 nm respectively and the volume corresponded to molecular weight of dimeric tARC6 (Figure 4-2, G).

In order to evaluate possible structural arrangement between FtsZ2, N-terminus and C-terminus of ARC6 during their interaction, two possible models representing coordinated interaction of FtsZ2 filament and ARC6 which also interact with C-terminal peptide of PDV2 (Figure 4-2, H). A model of full length FtsZ2 generated using Phyer2 server [103] and the protofilament model based on known structure (1W59) [104] were aligned with that of the tARC6 dimer in two possible orientations. Crystal structure of C-terminal domains of ARC6-PDV2 complex was also shown on the top which aligned well with transmembrane domain models of ARC6 and 3D reconstruction of ARC6. These models show the distance between two ARC6 domains were close to the distance of two FtsZ2 subunits and that of two C-terminal domain of ARC6 (Figure 4-2, H).

Figure 4-2. 3D reconstruction of dimeric tARC6 and model for FtsZ2 binding. (A) Raw image of negatively stained protein particles. Scale bar corresponds to 50 nm. (B) Representative raw particles, (C) Representative class averages, (D) Back projections from 3D reconstruction are shown. Scale bar corresponds to 5 nm. (E) Fourier shell correlation of 8 iterations and 0.5 FSC corresponds to approximately 22 Å. (F) asymmetric triangle of final reconstruction representing projection of all Euler angles (G) Front and tilted view of 3D reconstruction of dimeric tARC6. (H) Two possible binding models of ARC6 on FtsZ2 protofilaments. Models of FtsZ2 protofilament with bound dimeric tARC6 and C-terminal domain of ARC6 (green) complexed with C-terminus of PDV2 (red) are shown. Transmembrane domain of ARC6 (gray) is generated and aligned with C-terminal of CTD of ARC6. C-terminus of FtsZ2 is indicated by an arrow.

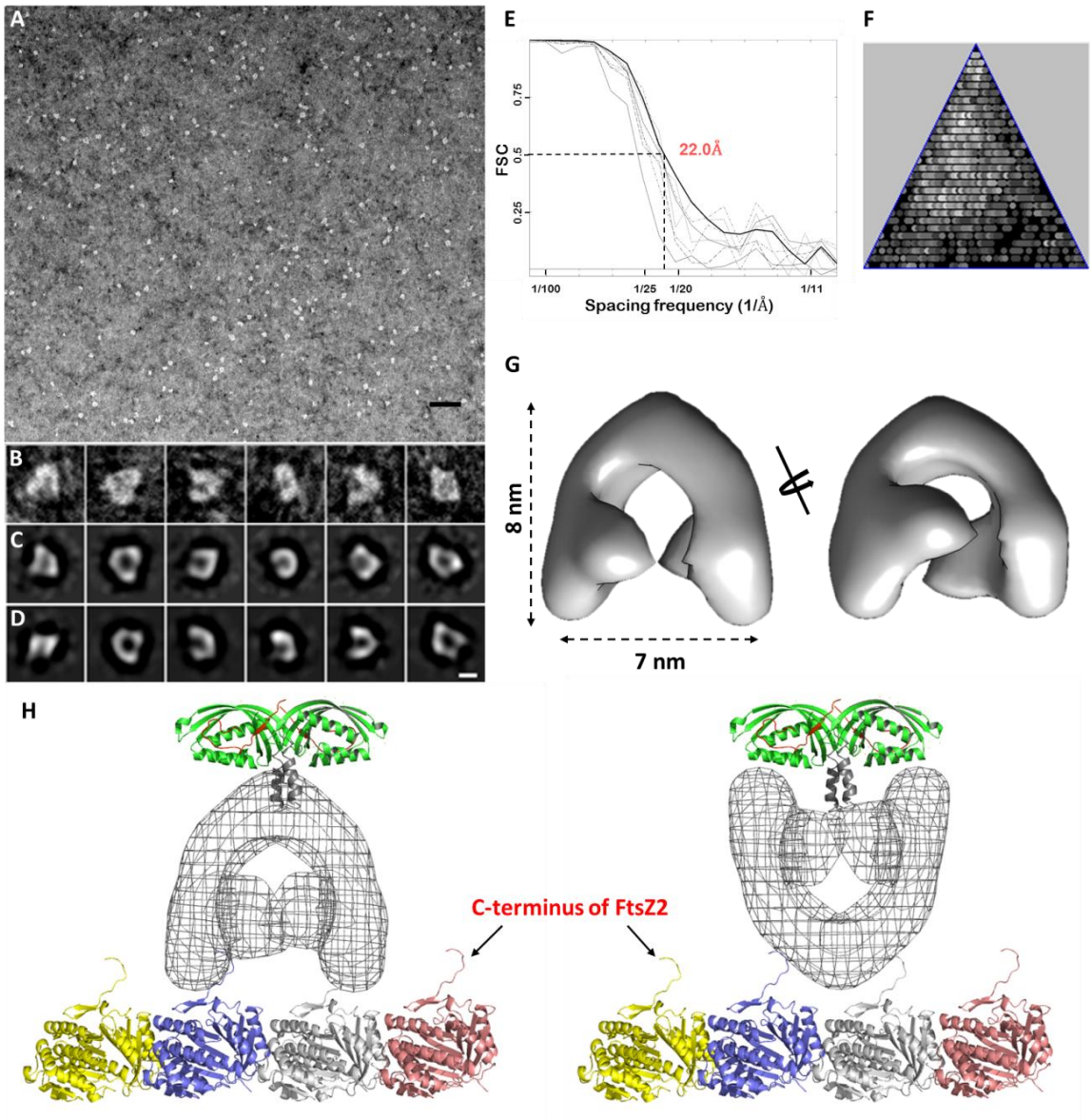
A
B
C
D
E
FSC
0.75
0.5
0.25
22.0Å
1/100
1/25
1/20
1/11
Spacing frequency (1/Å)
F
G
8 nm
7 nm
H
C-terminus of FtsZ2

4.3 DISCUSSION

Negatively stained tARC6 proteins imaged on TEM showed and confirmed its dimeric form. Smaller particles were rarely observed and these are possibly monomeric tARC6 unresolved from gel permeation chromatography. Three-dimensional reconstruction of tARC6 appeared as horse-shoe shape and the location and orientation of N-terminal and C-terminal portion of tARC6 and their interacting region are still unclear. However, interestingly, the reconstructed model has shown that the length and width of dimeric tARC6 aligned well with the distances of two FtsZ2 units and two of transmembrane domains linked to C-terminal domains of ARC6 in both possible binding models (Figure 4-2, H). Previous results from our study have shown that tARC6 does not cross links FtsZ2 filaments (Figure 2-5, B, C) and prevents immediate dissociation of FtsZ2 from disassembly condition (Figure 3-2). These results suggests that tARC6 binds to FtsZ2 subunits in cooperated in one strand in a longitudinal direction as shown in the binding model (Figure 4-2, H). Structural elucidation of FtsZ2- tARC6 complex may solve these questions and fully define its structure and functional role in chloroplast division.

4.4 EXPERIMENTAL PROCEDURES

4.4.1 3D reconstruction

Dimeric tARC6 was purified as described above and fresh specimens (80 μg/ml) were prepared according to Valentines et al.[105] and negatively stained using an aqueous solution of 2% uranyl acetate. Specimens were observed in a JEOL 1200 EX TEM operated at an accelerating voltage of 100 kV. Images were captured at calibrated

magnifications using an optically coupled 3 k slow scan CCD camera (model 15C, SIA, Duluth, GA) and Maxim DL imaging software resulting at 0.51 nm/pixel. Suitable micrographs (absence of drift, astigmatism, etc.) were selected and the Boxer program in EMAN 1.9 was used to hand pick 4121 particles from micrographs with similar defocus values. Particles were further processed by bandpass-filter to remove special frequencies below 11 A˚and above 100 A˚. Reference-free classification was performed by multivariate statistical analysis and hierarchical ascendant classification within the framework of the EMAN software package [106]. Initial model was generated by cross common lines euler search performed on class averages. The angular refinement iteration was performed using C2 symmetry and stopped when no further improvement of resolution was observed. The refinement procedure was repeated using the same starting model and C1 symmetry, to check for symmetry artefacts. The resulting reconstruction in C1 appeared as horse-shoe shape similar to the model produced via refinement with C2 symmetry imposed. Resolution was estimated by Fourier shell correlation (FSC) using the 0.5 criterion [107]. Three-dimensional reconstruction was manipulated and visualized using Chimera software package [108].

4.4.2 Generation of model of FtsZ2 protofilaent

FtsZ2 model was generated Phyre2 server [103] with *Microbacterium tuberculosis* FtsZ (1RLU) as a template. And the straight protofilament model was created manually based on known the FtsZ protofilament structure from *Methanocaldococcus jannaschii* (1W59) [104] and visualized using PyMOL (http://www.pymol.sourceforge.net).

CHAPTER V

CONCLUSION AND FUTURE STUDY

5.1 CONCLUSION

The research described here allows for a few contributions to the literature in the field of plastid division and advances in the *in vitro* assays for biochemical characterization of proteins involved in the plastid division machinery. Prior to this work, FtsZ1 and FtsZ2 proteins were expressed in a bacterial system in the insoluble fraction [42], or FtsZ proteins, ARC6 and PARC6 were expressed in a heterologous expression system [43, 59] which did not allow for a biochemical characterization *in vitro*. The proteins from our constructs and expression system, our laboratory provided evidences that FtsZ2 and ARC6 proteins were expressed as dimer. And biochemical characterization of these proteins was conducted *in vitro*. Evidence is provided that tARC6 exists as a dimer upon purification and co-localizes on FtsZ2 filaments affecting FtsZ2 assembly by interaction with the C-terminal tail of FtsZ2 (Figure 2-3, 2-4) in agreement with published results on the C-terminal tail of FtsZ2 [27, 53, 54, 59, 61] . Our results have shown that tARC6 affects FtsZ2 assembly without forming higher ordered FtsZ filament structures unlike bacterial FtsZ positive regulators [64, 73, 74, 76-78]. Chapter III describes research that investigates how tARC6 affects FtsZ2 assembly using FRAP and light scattering experiments in variable conditions. Our data have shown tARC6 prevented GDP induced FtsZ2 disassembly and has shown significant effect on FtsZ2 assembly when GDP was present (Figure 2-6, 3-1, 3-2). And this is not achieved by modulation of

GTPase activity of FtsZ2 (Figure 3-4, A). Interestingly, our data have shown that tARC6 affect FtsZ2 assembly significantly when GDP is present (Figure 3-4, B, C). Together, we conclude that tARC6 prevents disassembly of GDP bound form of FtsZ2 subunits thereby facilitate assembly and reduce the dynamics of FtsZ2. The 3D reconstruction of tARC6 shows a horse-shoe like dimeric molecule and provided clues for possible interactions between FtsZ filaments-ARC6-PDV2 essential to co-ordinate inner and outer contractile rings at the division site.

5.2 Effect of dimerization of ARC6 on Z-ring formation and coordination of PDV2

ARC6 is known as an FtsZ-stabilizing factor and to anchor the FtsZ filaments to the inner envelope membrane via direct interaction with conserved C-terminal tail of FtsZ2 [27, 54, 61]. Our data has shown that tARC6 prevents immediate disassembly of FtsZ2 filaments thereby facilitate assembly without membrane tethering function *in vitro*. Another key role of ARC6 in the chloroplast is coordinating localization of inner ring and outer ring across the two membranes by interaction with C-terminus of PDV2 which is known to recruit DRP5B and FtsZ2 [1, 26, 27]. A recent study has shown that C-terminal peptide, especially V281-I291, of PDV2 interacts with and induces dimer of conserved C-terminal domain of ARC6 [28]. While previous study has shown G307 of C-terminus of PDV2 as a key residue for interaction with ARC6 [27] , R288 from the C-terminus of PDV2 has shown a significant effect on interaction with ARC6 in the recent study and proposed that G307 anchors C-terminal peptide of PDV2 inside of C-terminal domain of ARC6 and R228 induces dimerization [28]. N-terminal portion of ARC6 (76-

618) exists as monomer in their experiment and suggested PDV2 induced dimerization of ARC6 in plastid as appeared in their crystal structure of C-terminal domain of ARC6-C complexed with C-terminal peptide of PDV2 (PDB ID: 5GTB) [28].

In our study, reducing agents were added to tARC6 proteins only after Ni-NTA columns as tARC6 included 5 cysteines, however reducing agent was removed at the final purification step and tARC6 appeared as a dimer from gel permeation chromatograph using Superose6 column equilibrated with the assembly buffer (50 mM HEPES pH 7.5, 100 mM KCl). To test if the protein also form monomers as with previous data where the N-terminal portion of ARC6 (76-618) formed monomer in a buffer containing 5 mM DTT [28], tARC6 was purified in an identical buffer. Preliminary data revealed that tARC6 in its reduced state can form monomers suggesting that cysteine residues are involved in dimerization (Figure 5-1).

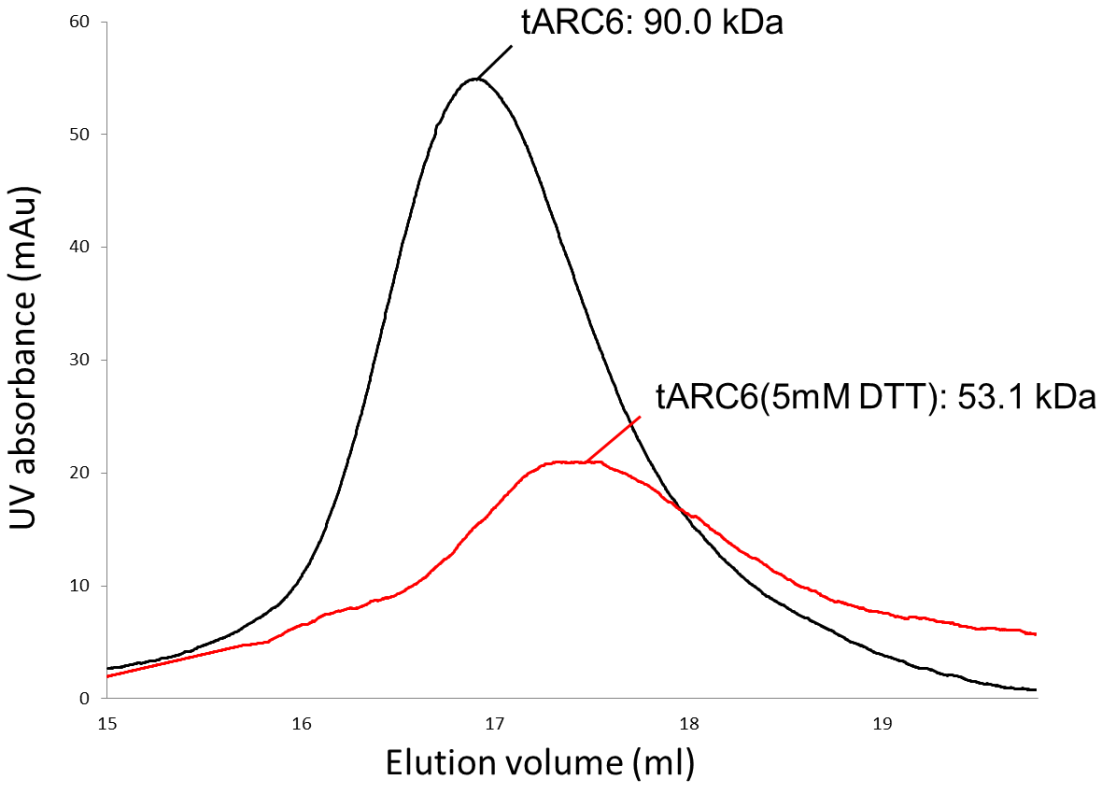

Figure 5-1. Dimer-monomer transition of tARC6 in a reducing environment. Gel permeation chromatography of t ARC6 in assembly buffer (black) and the same buffer with reducing agent (red) are shown from Superose 6 column. The estimated molecular mass corresponding to each protein is indicated.

It is possible that self-association of ARC6 is depends on reduction and oxidation status of thiol groups in light mediated redox system of the chloroplast. As previously known, activity of some enzymes in stroma is affected by pH and redox system which are regulated by light, so the chloroplast can switch between dark and light metabolism [72, 109-111]. Studies also have shown that the division and growth of chloroplast in the leaf cells are stimulated in light than in darkness and depend on light [112, 113] indicating light dependent regulation of chloroplast division. Together with our data, ARC6

possibly form dimer or monomers depend on redox condition in stroma and show different level of activity regarding interaction with FtsZ filaments and PDV2. Therefore, it would be important to test if the reducing condition affects dimeric formation of ARC6 and interaction with C-terminus of PDV2 and if the monomeric ARC6 maintains its role in facilitation of FtsZ2 assembly. Our hypothesis is that ARC6 forms monomer in reducing environment and showing different oligomeric status depend on light regulated redox condition in stroma. In our preliminary experiments, the assembly of FtsZ2 was not affected by presence of 5 mM DTT (data not shown) in our system. So, with our current protein constructs and assay systems, the effect of monomeric tARC6 in the presence of reducing agent could be tested by monitoring light scattering of FtsZ2 as in our study. To be consistent with our light scattering experiments, the same amount of tARC6 would be used to test if dimerization is the only factor in this compensatory light scattering assay.

Furthermore, it would be crucial to test if dimeric form of full length ARC6 has a different affinity to the C-terminal peptide of PDV2. It was previously shown that the synthetic polypeptide PDV2 (282–307) exhibits a binding affinity to monomeric ARC (6646–801) with a Kd of 46 μM, i.e. representing a relatively weak affinity [28]. However, it is possible that the dimeric form of ARC6 may bind to the polypeptide PDV2282–307 more tightly. Previous studies of DNA-binding proteins and other enzymes have shown that dimerization could give significantly higher affinities towards their counter partners or ligands [114-116]. From our preliminary experiments, full-length ARC6 (81.7 kDa) was purified as a soluble fraction and formed dimers in same

purification scheme used for tARC6 (see Methods). Freshly purified dimeric full-length ARC6 (Figure 5-2, A-C) was negatively stained and imaged using TEM, and then images were processed further as described in the 3D reconstruction of tARC6 leading to class averages of full-length ARC6 that shared morphologies similar to those observed with tARC6 (Figure 5-2, D-F).

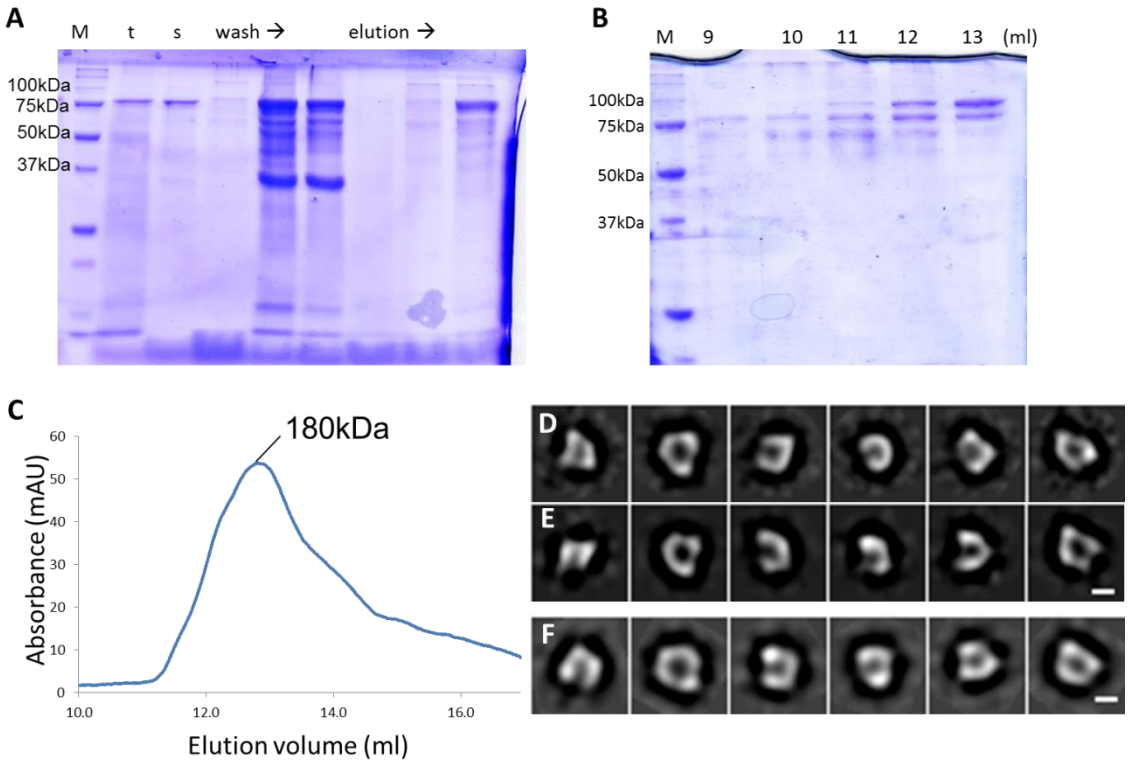

Figure 5-2. Purification of full length ARC6 and class averages of negatively stained full-length ARC6 protein particles. Fractions from Ni-NTA column (A) and Superose 6 gel permeation chromatography column (B) were analyzed by 15% SDS-PAGE gel respectively. Elution profile (C) and its corresponding molecular weight is shown. (D) Representative class averages and (E) Back projections from 3D reconstruction of tARC6 are shown for comparison. Scale bar corresponds to 5 nm. (F) Representative class averages of full-length ARC6 is shown. Scale bar corresponds to 5 nm.

5.3 Role of ARC6 during the transition of plastid division from ring formation to constriction

During the process of plastid division, ARC6 facilitates the Z-ring formation and disappears at the separation step while PDV1 and PARC6 were detected at polar site of two daughter chloroplast cells [1, 11, 70] (Figure 1-1). However, how ARC6 plays a role throughout plastid division and when ARC6 is released from the division site are not known. Release of ARC6 and the following constriction of the Z-ring would be the key steps to fully understand the process of plastid division in terms of transition from positive to negative regulation of the Z-ring.

PARC6 is known to act in the division site downstream of ARC6 [11] and interact with conserved C-terminal tail including F466 of FtsZ2 similar to the interaction between ARC6 and FtsZ2. PARC6 was co-localized on FtsZ2 filaments without inhibiting FtsZ2 assembly [12]. These results open the possibility that PARC6 could compete with ARC6 on interaction with FtsZ2 and have a role in replacing ARC6 as an alternative Z-ring anchor to the membrane. Also, as ARC6 is released from the division site, interaction with PDV2 could be disrupted. Furthermore, by sequestering the MORN domain of ARC3 by PARC6, ARC3 become freer to interact with FtsZ filaments leading to increased ARC3 activity [12, 13]. So, in the absence of ARC6, ARC3 may show more significant effect on remodeling of Z-ring and initiates the inner ring constriction dramatically.

Another possibility is that ARC6 may dissociate from the Z-ring when ARC3 is recruited. And the plastid stops Z-ring formation at the separation phase. PARC6 is

known to tether Z-ring to the membrane as another additional anchoring protein and recruit ARC3 through interaction with MORN domain of ARC3 [11, 12, 61]. Accumulating data have revealed the possibility that ARC6 and PARC6 both anchor Z-ring to the inner membrane, while ARC3 gradually remodel and promote disassembly of Z-ring. In this case, it is possible that synchronized constriction of inner and outer ring would be processed by ARC3 and both PDV1 and PDV2 which is known to promote disassembly inner ring and outer ring respectively, while ARC6 and PARC6 both anchor and Z-ring to the inner envelope membrane.

This hypothesis could be tested by investigating competitive interaction of PARC6 and ARC6 proteins on FtsZ2 filaments. One of the simple experiments design is to show co-localization of these two proteins on FtsZ filaments and perform FRAP. Previously GFP-tARC6 showed co-localization on FtsZ2 filaments *in vitro* from our data (Figure 2-4). Since fluorescence protein tagged N-terminal portion of PARC6 could be expressed as reported [12], *in vitro* assay of tARC6 and PAC6 would be available in variable stoichiometric ratios. The experiment would be able to elucidate whether PARC6 can co-exist or compete with ARC6 on FtsZ2 filaments *in vitro*. Furthermore, for the FRAP experiment, fluorescence protein tagged stromal portions of PARC6 and ARC6 could be co-expressed with FtsZ2 proteins in *S. pombe* and the effect of PARC6 on turnover of ARC6 or vice versa could be investigated. This would confirm possible coexistence and the effect of PARC6 on ARC6 turnover from FtsZ2 filaments *in vivo*.

ARC6 is known to form a complex which corresponds to ~200~250 kDa and is comprised of FtsZ1, FtsZ2 and ARC3 [54] suggesting that ARC6 may work with FtsZ1,

FtsZ2 and ARC3 for modulation of filament dynamics during the constriction process. PARC6 was known to indirectly inhibit FtsZ assembly by recruitment of ARC3 [11, 12], however biochemical characterization of PARC6 and its effect on FtsZ2 assembly were not defined in combination with ARC6 and ARC3 proteins *in vitro*. Although most of regulatory proteins of FtsZ assembly in the chloroplasts are discovered, how plastid begins the constriction by releasing ARC6 and inhibiting FtsZ assembly during the recruitment of variable antagonistic proteins to the division site is unclear up to date. Using light scattering, FtsZ2 assembly could be monitored in the presence of combination of these regulatory proteins as shown in the Table 2 to reveal which factor affects FtsZ assembly and initiates constriction of Z-ring.

Table 2. FtsZ2 assembly in the presence of combinational regulatory protein mixtures.

	Proteins				Aims
	FtsZ2	ARC6	PARC6	ARC3	
1	+	-	-	-	Control 1: 2 μM FtsZ2 assembly initiated by 1 mM GTP
2	+	+	-	-	Control 2: effect of ARC6 on FtsZ2 assembly
3	+	-	+	-	Control 3: effect of PARC6 on FtsZ2 assembly
4	+	-	-	+	Control 4: effect of ARC3 on FtsZ2 assembly
5	+	-	+	+	Effect of PARC6 on ARC3 mediated FtsZ2 disassembly
6	+	+	+	-	Effect of PARC6 on ARC6 mediated FtsZ2 assembly
7	+	+	-	+	Effect of ARC3 on ARC6 mediated FtsZ2 assembly
8	+	+	+	+	Effect of PARC6 and ARC3 on ARC6 mediated FtsZ2 assembly

FtsZ2 assembly where all of regulatory proteins can show their effect *in vitro* will be used. The aims of each test are shown in the Table 2. For the tests 6-7, FtsZ2 assembly will be performed in the presence of indicated regulatory proteins and the results will be compared to test 2 (Table 2). Regarding the order of recruitment of regulatory proteins to the division site (Figure 1-1), significant reduce of FtsZ2 assembly would indicate a radical transition of plastid division toward constriction. PARC6 and ARC3 could show accumulative inhibitory effect of ARC6 mediated FtsZ2 assembly. Together with experiments of fluorescence protein tagged regulatory proteins and light scattering

experiments, question about how the effect of ARC6 on Z-ring formation reduces during recruitment of antagonistic regulatory proteins could be resolved.

REFERENCES

1. Osteryoung, K.W. and K.A. Pyke, Division and dynamic morphology of plastids. Annu Rev Plant Biol, 2014. 65: p. 443-72.

2. Yoshida, Y., et al., The plastid-dividing machinery: formation, constriction and fission. Curr Opin Plant Biol, 2012. 15(6): p. 714-21.

3. Miyagishima, S.Y., H. Nakanishi, and Y. Kabeya, Structure, regulation, and evolution of the plastid division machinery. Int Rev Cell Mol Biol, 2011. 291: p. 115-53.

4. Pyke, K.A., Plastid division and development. Plant Cell, 1999. 11(4): p. 549-56.

5. Okazaki, K., Y. Kabeya, and S.Y. Miyagishima, The evolution of the regulatory mechanism of chloroplast division. Plant Signal Behav, 2010. 5(2): p. 164-7.

6. Miyagishima, S.Y., et al., Two types of FtsZ proteins in mitochondria and red-lineage chloroplasts: the duplication of FtsZ is implicated in endosymbiosis. J Mol Evol, 2004. 58(3): p. 291-303.

7. Stokes, K.D. and K.W. Osteryoung, Early divergence of the FtsZ1 and FtsZ2 plastid division gene families in photosynthetic eukaryotes. Gene, 2003. 320: p. 97-108.

8. Stokes, K.D., et al., Chloroplast division and morphology are differentially affected by overexpression of FtsZ1 and FtsZ2 genes in *Arabidopsis*. Plant Physiol, 2000. 124(4): p. 1668-77.

9. Nogales, E., et al., Tubulin and FtsZ form a distinct family of GTPases. Nat Struct Biol, 1998. 5(6): p. 451-8.

10. Jarvis, P. and E. Lopez-Juez, Biogenesis and homeostasis of chloroplasts and other plastids. Nat Rev Mol Cell Biol, 2013. 14(12): p. 787-802.

11. Glynn, J.M., et al., PARC6, a novel chloroplast division factor, influences FtsZ assembly and is required for recruitment of PDV1 during chloroplast division in *Arabidopsis*. Plant Journal, 2009. 59(5): p. 700-711.

12. Zhang, M., et al., Roles of *Arabidopsis* PARC6 in Coordination of the Chloroplast Division Complex and Negative Regulation of FtsZ Assembly. Plant Physiol, 2016. 170(1): p. 250-62.

13. Zhang, M., et al., Chloroplast division protein ARC3 regulates chloroplast FtsZ-ring assembly and positioning in *Arabidopsis* through interaction with FtsZ2. Plant Cell, 2013. 25(5): p. 1787-802.

14. Arumugam, S., Z. Petrasek, and P. Schwille, MinCDE exploits the dynamic nature of FtsZ filaments for its spatial regulation. Proc Natl Acad Sci U S A, 2014. 111(13): p. E1192-200.

15. Szeto, T.H., et al., Membrane localization of MinD is mediated by a C-terminal motif that is conserved across eubacteria, archaea, and chloroplasts. Proc Natl Acad Sci U S A, 2002. 99(24): p. 15693-8.

16. Hu, Z. and J. Lutkenhaus, A conserved sequence at the C-terminus of MinD is required for binding to the membrane and targeting MinC to the septum. Mol Microbiol, 2003. 47(2): p. 345-55.

17. Zhou, H. and J. Lutkenhaus, The switch I and II regions of MinD are required for binding and activating MinC. J Bacteriol, 2004. 186(5): p. 1546-55.

18. Ghosal, D., et al., MinCD cell division proteins form alternating copolymeric cytomotive filaments. Nat Commun, 2014. 5: p. 5341.

19. Aldridge, C. and S.G. Moller, The plastid division protein AtMinD1 is a Ca2+-ATPase stimulated by AtMinE1. J Biol Chem, 2005. 280(36): p. 31673-8.

20. Hu, Z. and J. Lutkenhaus, Topological regulation of cell division in *E. coli*. spatiotemporal oscillation of MinD requires stimulation of its ATPase by MinE and phospholipid. Mol Cell, 2001. 7(6): p. 1337-43.

21. Hale, C.A., H. Meinhardt, and P.A. de Boer, Dynamic localization cycle of the cell division regulator MinE in *Escherichia coli*. Embo J, 2001. 20(7): p. 1563-72.

22. Hu, Z., E.P. Gogol, and J. Lutkenhaus, Dynamic assembly of MinD on phospholipid vesicles regulated by ATP and MinE. Proc Natl Acad Sci U S A, 2002. 99(10): p. 6761-6.

23. Nakanishi, H., et al., Plant-specific protein MCD1 determines the site of chloroplast division in concert with bacteria-derived MinD. Curr Biol, 2009. 19(2): p. 151-6.

24. Shimada, H., et al., ARC3, a chloroplast division factor, is a chimera of prokaryotic FtsZ and part of eukaryotic phosphatidylinositol-4-phosphate 5-kinase. Plant and Cell Physiology, 2004. 45(8): p. 960-7.

25. Yoshida, Y., et al., Chloroplasts divide by contraction of a bundle of nanofilaments consisting of polyglucan. Science, 2010. 329(5994): p. 949-53.

26. Gao, H., et al., ARC5, a cytosolic dynamin-like protein from plants, is part of the chloroplast division machinery. Proc Natl Acad Sci U S A, 2003. 100(7): p. 4328-33.

27. Glynn, J.M., J.E. Froehlich, and K.W. Osteryoung, *Arabidopsis* ARC6 coordinates the division machineries of the inner and outer chloroplast membranes through interaction with PDV2 in the intermembrane space. The Plant Cell, 2008. 20(9): p. 2460-70.

28. Wang, W., et al., Structural insights into the coordination of plastid division by the ARC6-PDV2 complex. Nat Plants, 2017. 3: p. 17011.

29. Miyagishima, S.Y., J.E. Froehlich, and K.W. Osteryoung, PDV1 and PDV2 mediate recruitment of the dynamin-related protein ARC5 to the plastid division site. Plant Cell, 2006. 18(10): p. 2517-30.

30. Vitha, S., et al., ARC6 Is a J-domain plastid division protein and an evolutionary descendant of the cyanobacterial cell division protein Ftn2. The Plant Cell, 2003. 15(8): p. 1918-1933.

31. Miyagishima, S.Y., C.P. Wolk, and K.W. Osteryoung, Identification of cyanobacterial cell division genes by comparative and mutational analyses. Mol Microbiol, 2005. 56(1): p. 126-43.

32. TerBush, A.D. and K.W. Osteryoung, Distinct functions of chloroplast FtsZ1 and FtsZ2 in Z-ring structure and remodeling. J Cell Biol, 2012. 199(4): p. 623-37.

33. Hanson, M.R. and A. Sattarzadeh, Stromules: recent insights into a long neglected feature of plastid morphology and function. Plant Physiol, 2011. 155(4): p. 1486-92.

34. Vitha, S., R.S. McAndrew, and K.W. Osteryoung, FtsZ ring formation at the chloroplast division site in plants. J Cell Biol, 2001. 153(1): p. 111-20.

35. Adams, D.W. and J. Errington, Bacterial cell division: assembly, maintenance and disassembly of the Z ring. Nature Reviews Microbiology, 2009. 7(9): p. 642-653.

36. Margolin, W., FtsZ and the division of prokaryotic cells and organelles. Nat Rev Mol Cell Biol, 2005. 6(11): p. 862-871.

37. Mukherjee, A. and J. Lutkenhaus, Guanine nucleotide-dependent assembly of FtsZ into filaments. J Bacteriol, 1994. 176(9): p. 2754-8.

38. Scheffers, D.J., et al., GTP hydrolysis of cell division protein FtsZ: evidence that the active site is formed by the association of monomers. Biochemistry, 2002. 41(2): p. 521-529.

39. Hsin, J., A. Gopinathan, and K.C. Huang, Nucleotide-dependent conformations of FtsZ dimers and force generation observed through molecular dynamics simulations. Proc Natl Acad Sci U S A, 2012. 109(24): p. 9432-7.

40. Li, Y., et al., FtsZ protofilaments use a hinge-opening mechanism for constrictive force generation. Science, 2013. 341(6144): p. 392-5.

41. Matsui, T., et al., Structural change in FtsZ Induced by intermolecular interactions between bound GTP and the T7 loop. J Biol Chem, 2014. 289(6): p. 3501-9.

42. Olson, B.J., Q. Wang, and K.W. Osteryoung, GTP-dependent heteropolymer formation and bundling of chloroplast FtsZ1 and FtsZ2. J Biol Chem, 2010. 285(27): p. 20634-43.

43. TerBush, A.D. and K.W. Osteryoung, Distinct functions of chloroplast FtsZ1 and FtsZ2 in Z-ring structure and remodeling. The Journal of Cell Biology, 2012. 199(4): p. 623-637.

44. TerBush, A.D., Y. Yoshida, and K.W. Osteryoung, FtsZ in chloroplast division: structure, function and evolution. Curr Opin Cell Biol, 2013. 25(4): p. 461-70.

45. Anderson, D.E., F.J. Gueiros-Filho, and H.P. Erickson, Assembly dynamics of FtsZ rings in *Bacillus subtilis* and *Escherichia coli* and effects of FtsZ-regulating proteins. J Bacteriol, 2004. 186(17): p. 5775-81.

46. Stricker, J., et al., Rapid assembly dynamics of *the Escherichia coli* FtsZ-ring demonstrated by fluorescence recovery after photobleaching. Proc Natl Acad Sci U S A, 2002. 99(5): p. 3171-5.

47. Chen, Y. and H.P. Erickson, FtsZ filament dynamics at steady state: subunit exchange with and without nucleotide hydrolysis. Biochemistry, 2009. 48(28): p. 6664-6673.

48. Alushin, G.M., et al., High-resolution microtubule structures reveal the structural transitions in alphabeta-tubulin upon GTP hydrolysis. Cell, 2014. 157(5): p. 1117-29.

49. Aylett, C.H., et al., Filament structure of bacterial tubulin homologue TubZ. Proc Natl Acad Sci U S A, 2010. 107(46): p. 19766-71.

50. Osteryoung, K.W., et al., Chloroplast division in higher plants requires members of two functionally divergent gene families with homology to bacterial ftsZ. The Plant Cell, 1998. 10(12): p. 1991-2004.

51. Yoder, D.W., et al., Effects of mutations in *Arabidopsis* FtsZ1 on plastid division, FtsZ ring formation and positioning, and FtsZ filament morphology *in vivo*. Plant and Cell Physiology, 2007. 48(6): p. 775-791.

52. Schmitz, A.J., et al., *Arabidopsis* FtsZ2-1 and FtsZ2-2 are functionally redundant, but FtsZ-based plastid division is not essential for chloroplast partitioning or plant growth and development. Molecular Plant, 2009. 2(6): p. 1211-1222

53. Maple, J., C. Aldridge, and S.G. Møller, Plastid division is mediated by combinatorial assembly of plastid division proteins. Plant Journal, 2005. 43(6): p. 811-823.

54. McAndrew, R.S., et al., *In vivo* quantitative relationship between plastid division proteins FtsZ1 and FtsZ2 and identification of ARC6 and ARC3 in a native FtsZ complex. Biochemical Journal, 2008. 412: p. 367-378.

55. Zhang, M., et al., Chloroplast Division Protein ARC3 Regulates Chloroplast FtsZ-Ring Assembly and Positioning in *Arabidopsis* through Interaction with FtsZ2. The Plant Cell, 2013. 25(5): p. 1787-1802.

56. Pyke, K.A., et al., arc6, A Fertile *Arabidopsis* Mutant with Only Two Mesophyll Cell Chloroplasts. Plant Physiol, 1994. 106(3): p. 1169-1177.

57. Pyke, K.A. and A.M. Page, Plastid ontogeny during petal development in *Arabidopsis*. Plant Physiol, 1998. 116(2): p. 797-803.

58. Robertson, E.J., K.A. Pyke, and R.M. Leech, arc6, an extreme chloroplast division mutant of *Arabidopsis* also alters proplastid proliferation and morphology in shoot and root apices. J Cell Sci, 1995. 108 (Pt 9): p. 2937-44.

59. TerBush, A.D., C.A. Porzondek, and K.W. Osteryoung, Functional Analysis of the Chloroplast Division Complex Using *Schizosaccharomyces pombe* as a Heterologous Expression System. Microsc Microanal, 2016. 22(2): p. 275-89.

60. Koksharova, O.A. and P.C. Wolk, A novel gene that bears a DnaJ motif influences cyanobacterial cell division. Journal of Bacteriology, 2002. 184: p. 5524-5528.

61. Johnson, C.B., et al., Single Particle Tracking Analysis of the Chloroplast Division Protein FtsZ Anchoring to the Inner Envelope Membrane. Microsc Microanal, 2013. 19(3): p. 507-512.

62. Marbouty, M., et al., ZipN, an FtsA-like orchestrator of divisome assembly in the model cyanobacterium Synechocystis PCC6803. Mol Microbiol, 2009. 74(2): p. 409-20.

63. Ajjawi, I., et al., A J-like protein influences fatty acid composition of chloroplast lipids in *Arabidopsis*. PLoS One, 2011. 6(10): p. e25368.

64. Durand-Heredia, J., et al., Identification of ZapD as a cell division factor that promotes the assembly of FtsZ in *Escherichia coli*. J Bacteriol, 2012. 194(12): p. 3189-98.

65. Feucht, A., et al., Cytological and biochemical characterization of the FtsA cell division protein of *Bacillus subtilis*. Mol Microbiol, 2001. 40(1): p. 115-25.

66. Dai, K. and J. Lutkenhaus, The proper ratio of FtsZ to FtsA is required for cell division to occur in *Escherichia coli*. J Bacteriol, 1992. 174(19): p. 6145-51.

67. Krol, E. and D.J. Scheffers, FtsZ polymerization assays: simple protocols and considerations. J Vis Exp, 2013(81): p. e50844.

68. Vaughan, S., et al., Molecular evolution of FtsZ protein sequences encoded within the genomes of archaea, bacteria, and eukaryota. J Mol Evol, 2004. 58(1): p. 19-29.

69. McAndrew, R.S., et al., Colocalization of plastid division proteins in the chloroplast stromal compartment establishes a new functional relationship between FtsZ1 and FtsZ2 in higher plants. Plant Physiol, 2001. 127(4): p. 1656-66.

70. Schmitz, A.J., et al., *Arabidopsis* FtsZ2-1 and FtsZ2-2 are functionally redundant, but FtsZ-based plastid division is not essential for chloroplast partitioning or plant growth and development. Mol Plant, 2009. 2(6): p. 1211-22.

71. Smith, A.G., et al., Oligomerization of plant FtsZ1 and FtsZ2 plastid division proteins. Arch Biochem Biophys, 2011. 513(2): p. 94-101.

72. Werdan, K., H.W. Heldt, and M. Milovancev, The role of pH in the regulation of carbon fixation in the chloroplast stroma. Studies on CO2 fixation in the light and dark. Biochim Biophys Acta, 1975. 396(2): p. 276-92.

73. Loose, M. and T.J. Mitchison, The bacterial cell division proteins FtsA and FtsZ self-organize into dynamic cytoskeletal patterns. Nat Cell Biol, 2014. 16(1): p. 38-46.

74. Kuchibhatla, A., A. Bhattacharya, and D. Panda, ZipA binds to FtsZ with high affinity and enhances the stability of FtsZ protofilaments. PLoS One, 2011. 6(12): p. e28262.

75. Pacheco-Gomez, R., et al., Tetramerization of ZapA is required for FtsZ bundling. Biochem J, 2013. 449(3): p. 795-802.

76. Singh, J.K., et al., SepF increases the assembly and bundling of FtsZ polymers and stabilizes FtsZ protofilaments by binding along its length. J Biol Chem, 2008. 283(45): p. 31116-24.

77. Huang, K.H., J. Durand-Heredia, and A. Janakiraman, FtsZ ring stability: of bundles, tubules, crosslinks, and curves. J Bacteriol, 2013. 195(9): p. 1859-68.

78. Goley, E.D., et al., Imaging-based identification of a critical regulator of FtsZ protofilament curvature in Caulobacter. Mol Cell, 2010. 39(6): p. 975-87.

79. El-Kafafi el, S., et al., The plastid division proteins, FtsZ1 and FtsZ2, differ in their biochemical properties and sub-plastidial localization. Biochem J, 2005. 387(Pt 3): p. 669-76.

80. Ward, J.E., Jr. and J. Lutkenhaus, Overproduction of FtsZ induces minicell formation in *E. coli*. Cell, 1985. 42: p. 941-949.

81. Dewar, S.J., K.J. Begg, and W.D. Donachie, Inhibition of cell division initiation by an imbalance in the ratio of FtsA to FtsZ. J Bacteriol, 1992. 174(19): p. 6314-6.

82. Mukherjee, A. and J. Lutkenhaus, Analysis of FtsZ assembly by light scattering and determination of the role of divalent metal cations. J Bacteriol, 1999. 181(3): p. 823-32.

83. Gaskin, F., C.R. Cantor, and M.L. Shelanski, Turbidimetric studies of the *in vitro* assembly and disassembly of porcine neurotubules. J Mol Biol, 1974. 89(4): p. 737-55.

84. Chen, Y., et al., Assembly dynamics of *Mycobacterium tuberculosis* FtsZ. J Biol Chem, 2007. 282(38): p. 27736-43.

85. Martos, A., et al., Isolation, characterization and lipid-binding properties of the recalcitrant FtsA division protein from *Escherichia coli*. PLoS One, 2012. 7(6): p. e39829.

86. Ma, X., D.W. Ehrhardt, and W. Margolin, Colocalization of cell division proteins FtsZ and FtsA to cytoskeletal structures in living *Escherichia coli* cells by using green fluorescent protein. Proc Natl Acad Sci U S A, 1996. 93(23): p. 12998-3003.

87. Beuria, T.K., et al., Adenine nucleotide-dependent regulation of assembly of bacterial tubulin-like FtsZ by a hypermorph of bacterial actin-like FtsA. J Biol Chem, 2009. 284(21): p. 14079-86.

88. Modi, K. and H.S. Misra, Dr-FtsA, an actin homologue in *Deinococcus radiodurans* differentially affects Dr-FtsZ and Ec-FtsZ functions *in vitro*. PLoS One, 2014. 9(12): p. e115918.

89. Fujita, J., et al., Crystal structure of FtsA from *Staphylococcus aureus*. FEBS Lett, 2014. 588(10): p. 1879-85.

90. RayChaudhuri, D., ZipA is a MAP-Tau homolog and is essential for structural integrity of the cytokinetic FtsZ ring during bacterial cell division. EMBO J, 1999. 18(9): p. 2372-83.

91. Hale, C.A., A.C. Rhee, and P.A. de Boer, ZipA-induced bundling of FtsZ polymers mediated by an interaction between C-terminal domains. J Bacteriol, 2000. 182(18): p. 5153-66.

92. Mosyak, L., et al., The bacterial cell-division protein ZipA and its interaction with an FtsZ fragment revealed by X-ray crystallography. EMBO J, 2000. 19(13): p. 3179-91.

93. Hale, C.A. and P.A. de Boer, Direct binding of FtsZ to ZipA, an essential component of the septal ring structure that mediates cell division in *E. coli*. Cell, 1997. 88(2): p. 175-85.

94. Liu, Z., A. Mukherjee, and J. Lutkenhaus, Recruitment of ZipA to the division site by interaction with FtsZ. Mol Microbiol, 1999. 31(6): p. 1853-61.

95. Chen, Y. and H.P. Erickson, Rapid *in vitro* assembly dynamics and subunit turnover of FtsZ demonstrated by fluorescence resonance energy transfer. J Biol Chem, 2005. 280(23): p. 22549-54.

96. Lu, C., M. Reedy, and H.P. Erickson, Straight and curved conformations of FtsZ are regulated by GTP hydrolysis. J Bacteriol, 2000. 182(1): p. 164-70.

97. Huecas, S. and J.M. Andreu, Polymerization of nucleotide-free, GDP- and GTP-bound cell division protein FtsZ: GDP makes the difference. FEBS Lett, 2004. 569(1-3): p. 43-8.

98. Small, E. and S.G. Addinall, Dynamic FtsZ polymerization is sensitive to the GTP to GDP ratio and can be maintained at steady state using a GTP-regeneration system. Microbiology, 2003. 149(Pt 8): p. 2235-42.

99. Smith, A.G., et al., Plant FtsZ1 and FtsZ2 expressed in a eukaryotic host: GTPase activity and self-assembly. FEBS Letters, 2010. 584(1): p. 166-172.

100. Maundrell, K., nmt1 of fission yeast. A highly transcribed gene completely repressed by thiamine. J Biol Chem, 1990. 265(19): p. 10857-64.

101. Bolte, S. and F.P. Cordelieres, A guided tour into subcellular colocalization analysis in light microscopy. J Microsc, 2006. 224(Pt 3): p. 213-32.

102. Lewis, B.A. and D.M. Engelman, Lipid bilayer thickness varies linearly with acyl chain length in fluid phosphatidylcholine vesicles. J Mol Biol, 1983. 166(2): p. 211-7.

103. Kelley, L.A., et al., The Phyre2 web portal for protein modeling, prediction and analysis. Nat Protoc, 2015. 10(6): p. 845-58.

104. Oliva, M.A., S.C. Cordell, and J. Lowe, Structural insights into FtsZ protofilament formation. Nat Struct Mol Biol, 2004. 11(12): p. 1243-50.

105. Valentine, R.C., B.M. Shapiro, and E.R. Stadtman, Regulation of glutamine synthetase. XII. Electron microscopy of the enzyme from *Escherichia coli*. Biochemistry, 1968. 7(6): p. 2143-2152.

106. Ludtke, S.J., P.R. Baldwin, and W. Chiu, EMAN: semiautomated software for high-resolution single-particle reconstructions. J Struct Biol, 1999. 128(1): p. 82-97.

107. Saxton, W.O. and W. Baumeister, The correlation averaging of a regularly arranged bacterial cell envelope protein. J Microsc, 1982. 127(Pt 2): p. 127-38.

108. Pettersen, E.F., et al., UCSF Chimera--a visualization system for exploratory research and analysis. J Comput Chem, 2004. 25(13): p. 1605-12.

109. Schurmann, P. and B.B. Buchanan, The ferredoxin/thioredoxin system of oxygenic photosynthesis. Antioxid Redox Signal, 2008. 10(7): p. 1235-74.

110. Meyer, Y., et al., Thioredoxins and glutaredoxins: unifying elements in redox biology. Annu Rev Genet, 2009. 43: p. 335-67.

111. Hauser, M., et al., Stimulation by Light of Rapid pH Regulation in the Chloroplast Stroma *in Vivo* as Indicated by CO2 Solubilization in Leaves. Plant Physiol, 1995. 108(3): p. 1059-1066.

112. Hashimoto, H. and J.V. Possingham, Effect of light on the chloroplast division cycle and DNA synthesis in cultured leaf discs of spinach. Plant Physiol, 1989. 89(4): p. 1178-83.

113. Chaly, N., J.V. Possingham, and W.W. Thomson, Chloroplast division in spinach leaves examined by scanning electron microscopy and freeze-etching. J Cell Sci, 1980. 46: p. 87-96.

114. Miyamoto, T., S. Suzuki, and L.J. DeGroot, High affinity and specificity of dimeric binding of thyroid hormone receptors to DNA and their ligand-dependent dissociation. Mol Endocrinol, 1993. 7(2): p. 224-31.

115. Lim, K.H., et al., Engineered streptavidin monomer and dimer with improved stability and function. Biochemistry, 2011. 50(40): p. 8682-91.

116. Marianayagam, N.J., M. Sunde, and J.M. Matthews, The power of two: protein dimerization in biology. Trends Biochem Sci, 2004. 29(11): p. 618-25.